



Rensselaer

MANE 4140: Intro Computational Fluid Dynamics

Final Project

Spring 2025

Liron Alishahian, Paul Khoury, Ryan Rebetti

Section	Contributor(s)
Overall Problem Description	LA(50%), RR(50%)
Problem Setup	PK(50%), RR(50%)
Numerical Scheme/Mesh Setup	LA(50%), PK(50%)
Other Details	PK(100%)
Results	LA(50%) RR (50%)
Closing Remarks	LA (33%), PK(33%), RR (33%)
TOTAL CONTRIBUTION	LA(35%), PK(35%), RR(30%)

Section 1: Overall problem description

This report will analyze the properties of a stacked airfoil consisting of three separate Selig 1223 airfoils. The S1223 airfoil has a high camber, which enhances lift (or downforce in the case of a car). In the automotive realm, this airfoil has been adapted by engineers aiming to enhance motorsport vehicle performance, particularly in generating downforce. For instance, a custom wing utilizing the S1223 airfoil was crafted for a Hyundai Veloster N to improve its balance.

The S1223 airfoil has been the subject of several computational studies in motorsport. The S1223 airfoil is not commonly employed in mass-produced vehicles; the stacked configuration is rarer still, with its use typically confined to custom or experimental projects. Our primary goal is to analyze its lift and drag coefficients in a stacked configuration. For the midterm project submission, we analyzed the airfoil with turbulent flow. For the final project, we will explore the **Turbulent flow** regime on a **stacked configuration** while also adding specific **mesh refinement** zones for a more accurate simulation and to improve resolution around areas of interest.

Equations: The simulation was based on the steady-state, incompressible flow equations.

Material inputs:

Air Properties at 40° C:

- Density: 1.127 kg/m³
- Dynamics viscosity: 1.918e-5 kg/m*s
- These values were chosen as they are the properties of air to correspond to air temperature above the track in racing conditions, as F1 events are often held in areas such as Texas, Australia, or Bahrain. The climate of these regions, coupled with the fact that track temperatures increase dramatically due to tire friction during a race, led us to select this temperature and the corresponding air properties at this temperature.

Conditions:

Reynolds number was computed given a velocity of 30 m/s and given the above material properties using the equation:

$$Re = \frac{\rho UL}{\mu}$$

Where ρ is fluid density, U is freestream velocity, L is chord length and μ is dynamic viscosity. Reynolds number was found to be $\sim 6.17e5$, indicating that it is in the turbulent regime for external flow. The resulting Mach number is ~ 0.085 , indicating that we are firmly in the subsonic regime. It is also important to note that for the stacked geometry, each airfoil will technically possess its own Reynolds number given varying chord lengths ($@c=0.175 Re \sim 3.1e5$, $@c=0.105 Re \sim 1.9e5$). However, when we discuss overall flow regime it is logical to refer to the main chord length.

Real data for validation: *Experimental Data from literature for Validation.*

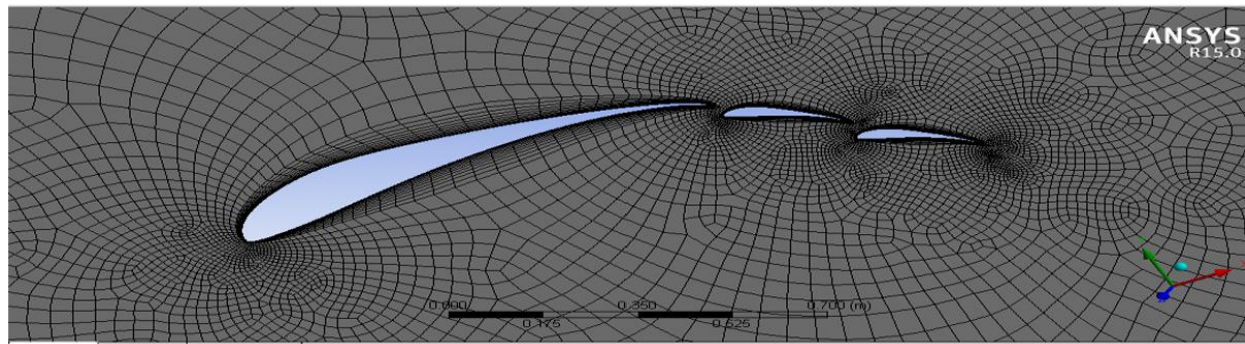
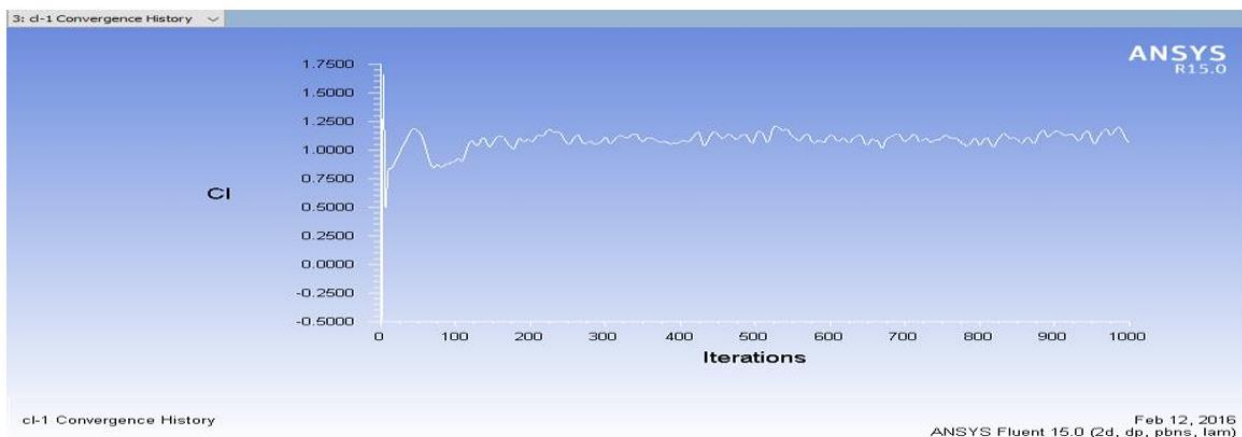
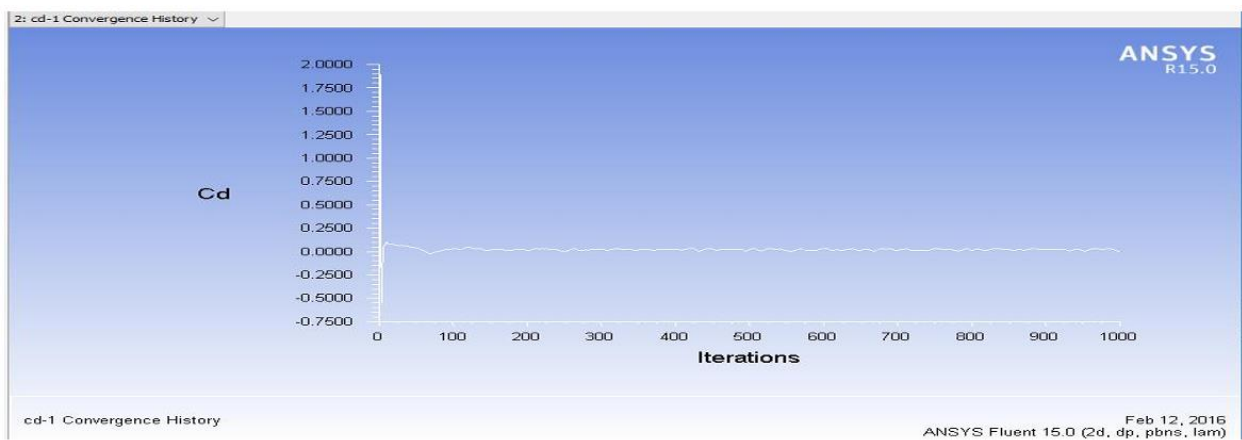


Fig 3 Airfoil S1223 With 2 Elements

Multi-Element S1223 Airfoil Geometry (from Ambhore and Mali 2016)



(1)



(2)

Expected Lift (1) and Drag (2) Coefficient Values for Stacked System

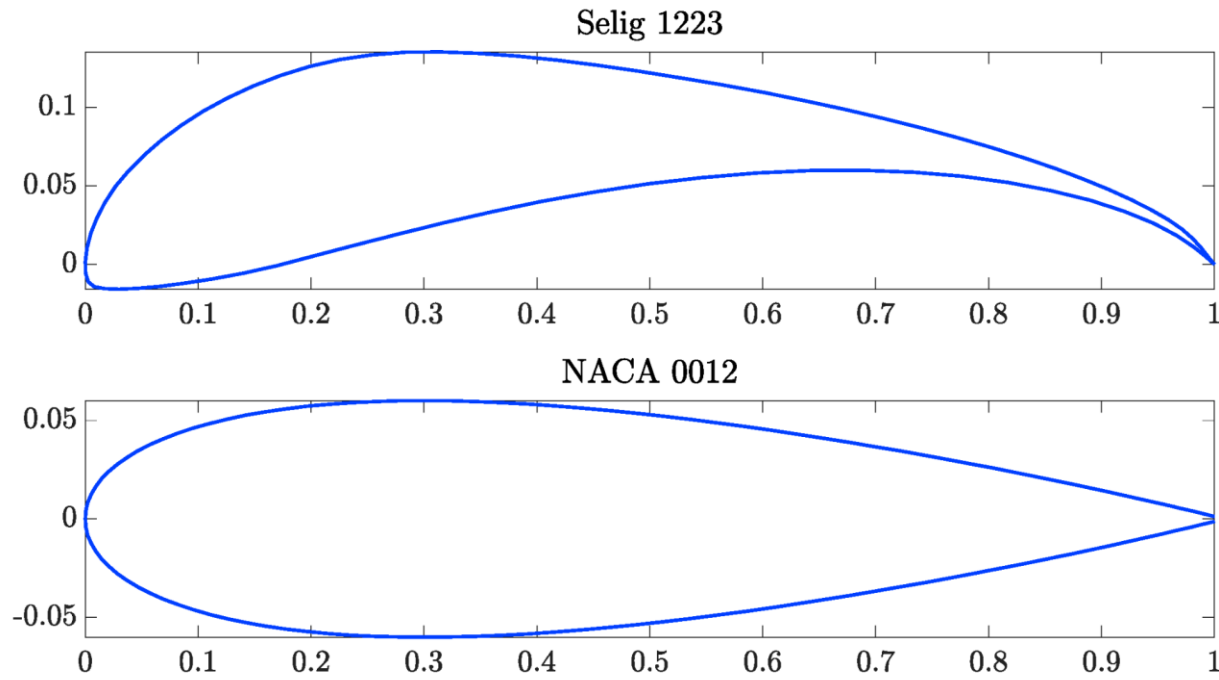
The above images are from *Multi Element Wing Analysis* [7]. It can be seen that the offset angle between airfoils in this setup is significantly lower than our geometry shown in section 2. As a

result, the expected drag coefficient will certainly be lower than our results while our lift coefficients may match up due to certain geometric similarities.

Section 2: Problem setup

Geometry:

The image below shows the comparison of a typical NACA 0012 (symmetrical airfoil) in comparison to the selected Selig 1223 (cambered airfoil) and their respective chord length proportions.



Section 2, Figure 1: Selig 1223 Airfoil geometry vs NACA 0012

The image below displays the geometry as it appeared after being imported into the simulation environment. Since the objective of this analysis is to assess the airfoil's performance in an automotive context—specifically for downforce generation—the airfoil is modeled in an “inverted” orientation, which is standard in racing applications. In such configurations, increasing angles of rotation for the higher airfoils are commonly employed, and this was reflected in the simulated setup.

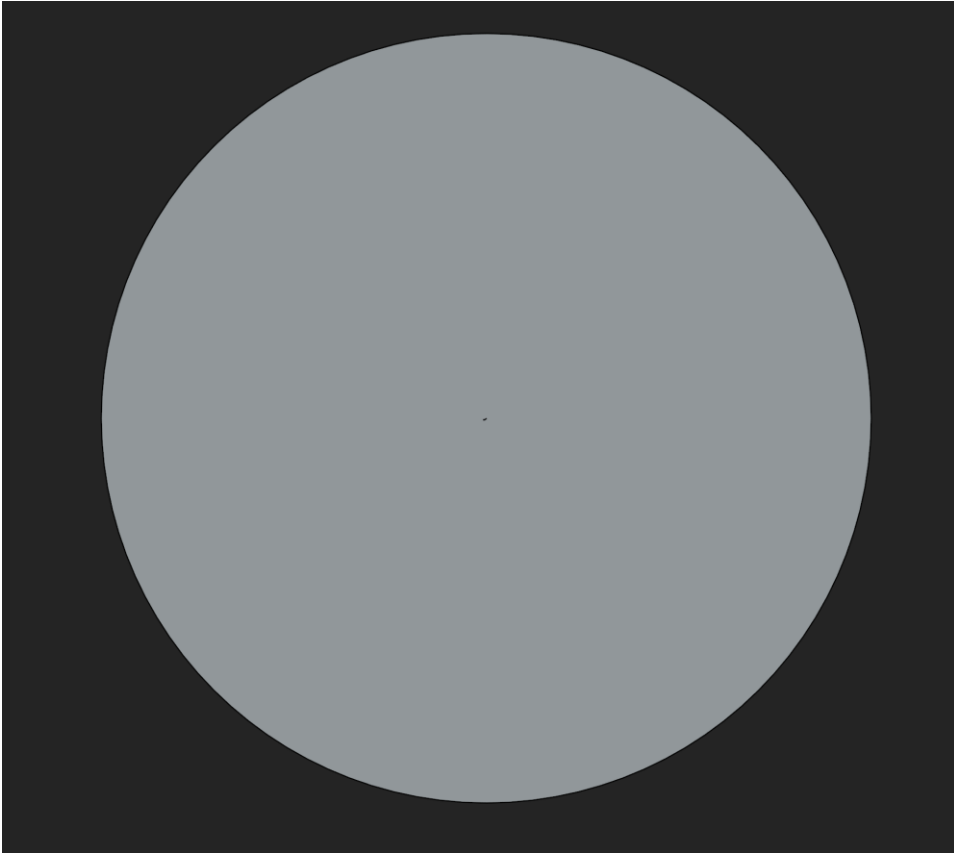
The system consists of three stacked airfoils. The first, or bottom airfoil, has a chord length C_1 of 0.35 meters (350 mm) and is angled at 7 degrees. The second airfoil is positioned directly above the first and has a chord length C_2 equal to $0.5C_1$ of the first, or 0.175 meters (175 mm), with an angle of attack of 28 degrees. The third and topmost airfoil has a chord length C_3 equal to $0.3C_1$ of the first airfoil, or 0.105 meters (105 mm), and is set at an angle of 46 degrees. Due to the overlapping arrangement of the airfoils, the total projected chord length, C_{total} , is 0.56 meters (560 mm), which is slightly less than the sum of the individual chord lengths.

The proportions and configuration of these airfoils were selected based on values cited in relevant literature, where similar geometries are used for rear wing assemblies in performance race cars.

The full model was placed in a far-field domain with a diameter of 70 meters, corresponding to 200 times the base chord length, to minimize boundary effects. The thickness of the flow domain was defined as one-fifth of the chord length, or 0.07 meters (70 mm), to properly capture boundary layer development while maintaining computational efficiency.



Section 2, Figure 2: Simplified Geometry Close-up



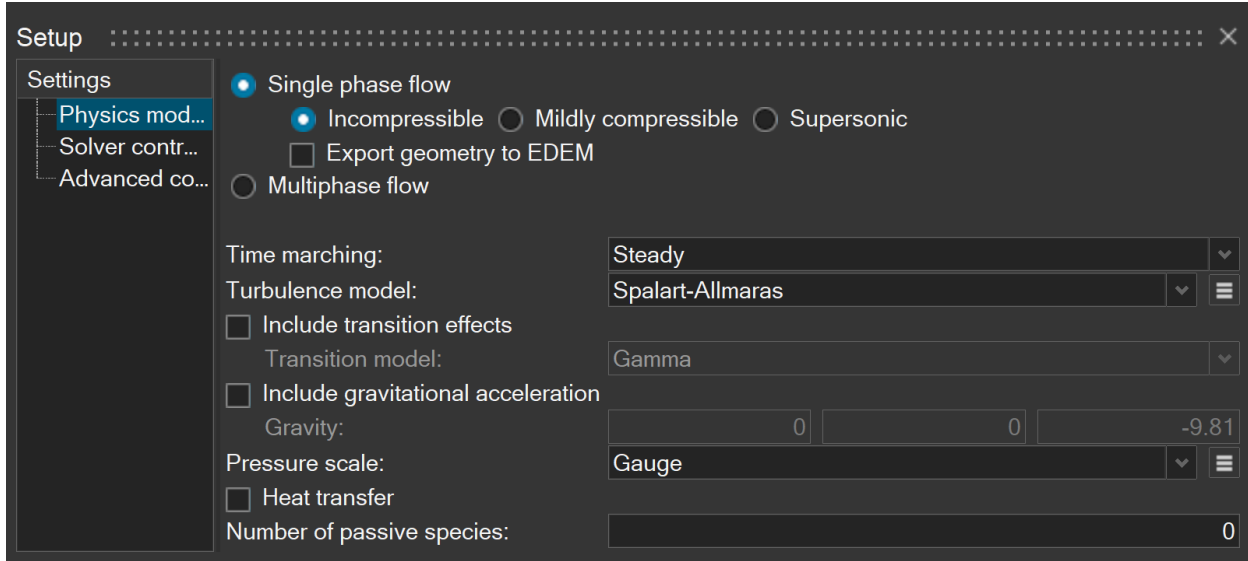
Section 2, Figure 3: Simplified Geometry full view (far field)

Physics:

The simulation was conducted as a steady-state analysis. While a transient analysis may have better replicated certain aspects of race-day conditions, we opted for a steady-state approach because another aspect of our setup, the far-field boundary conditions (BCs), does not work well with a transient analysis. Furthermore, the additional computational time and resources required for a transient simulation were not within the scope of the project.

Computational Model:

We used the Spalart–Allmaras turbulence model was used for this simulation. It is a one-equation model based on the Reynolds-Averaged Navier–Stokes (RANS) equations and is particularly well-suited for capturing turbulent flow in external aerodynamic applications. Its computational ability to model boundary layer behavior makes it an appropriate choice for this study.



Section 2, Figure 4: Physics Setup

Boundary Conditions:

The simulation was conducted with an airflow velocity of 30 m/s in the positive x-direction under atmospheric pressure conditions. No-slip conditions were applied to all surfaces of the airfoil cut-out (6 surfaces total, 2 from each airfoil). Additionally, symmetry boundary conditions were imposed on the flat sides of the far-field disk.

Resource Allocation and Focus on the Middle Element:

Due to the high computational cost of resolving fine-scale flow interactions across all three airfoil elements at our target resolution, we chose to concentrate on a select “area of interest” - the second (middle) airfoil only. In a multi-element stack, the middle element experiences the most complex interference effects, both from the leading element’s wake and from other effects from the trailing tip. By dedicating our available CPU hours and memory budget to this section, we were able to accurately capture the behavior of interest surrounding it.

Specifically, this focus provided three key benefits:

1. It captures the strongest flow interactions around the middle airfoil without overloading the solver.
2. It still reflects the main stacking effects, since disturbances here influence the rest of the wing.
3. It lets us obtain reliable lift, drag, and boundary-layer results within our available time and compute budget.

For these reasons, only the middle airfoil had an Edge Layer Mesh.

Section 3: Numerical scheme & Mesh setup & Time integration

Numerical scheme:

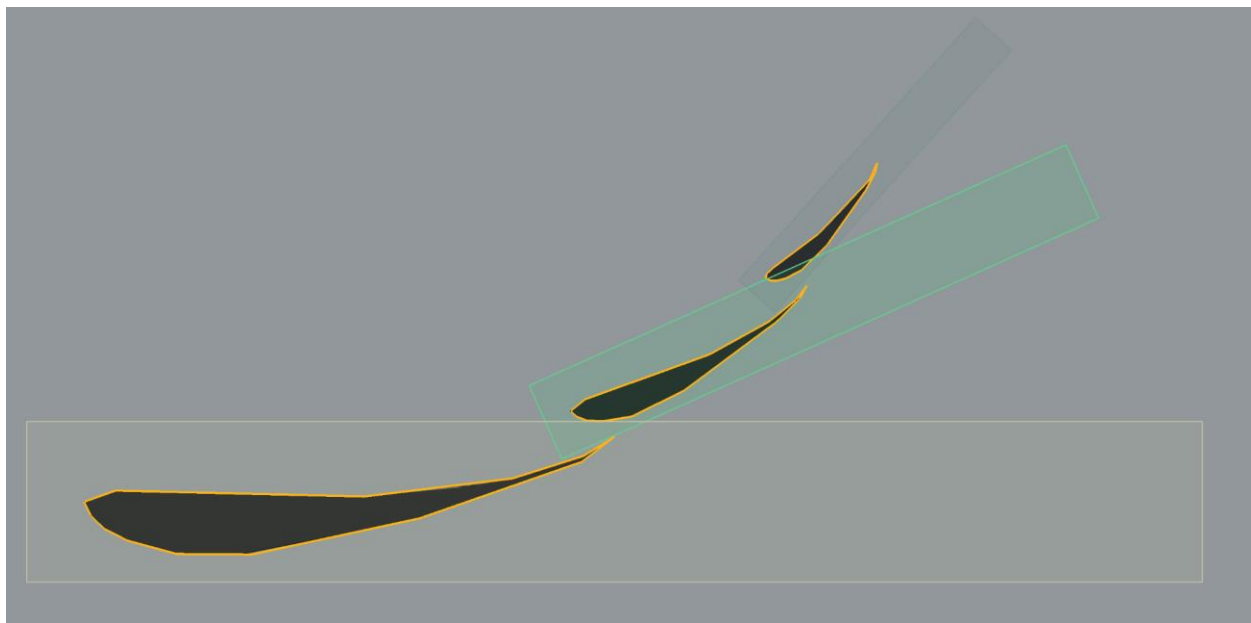
All simulations were conducted using default AcuSolve settings

Time integration details:

No time integration details were present as this was a steady-state analysis.

Mesh setup:

First, an edge mesh was defined, with the Average element size set to the length of $C_{1,2,3}/128$ for each individual chord length. The edge layer mesh's first layer thickness was set to $C_{1,2,3}/10,000$, ensuring a fine resolution near the boundary layer for each individual airfoil. The mesh consists of a total of 24 layers, with a constant growth method and a constant growth rate of 1.2 to maintain uniformity in the layer expansion. The termination policy was set to 'Truncate' to avoid excessive layer growth. Surface mesh modifications were enabled to refine the mesh near the surface and improve overall accuracy.



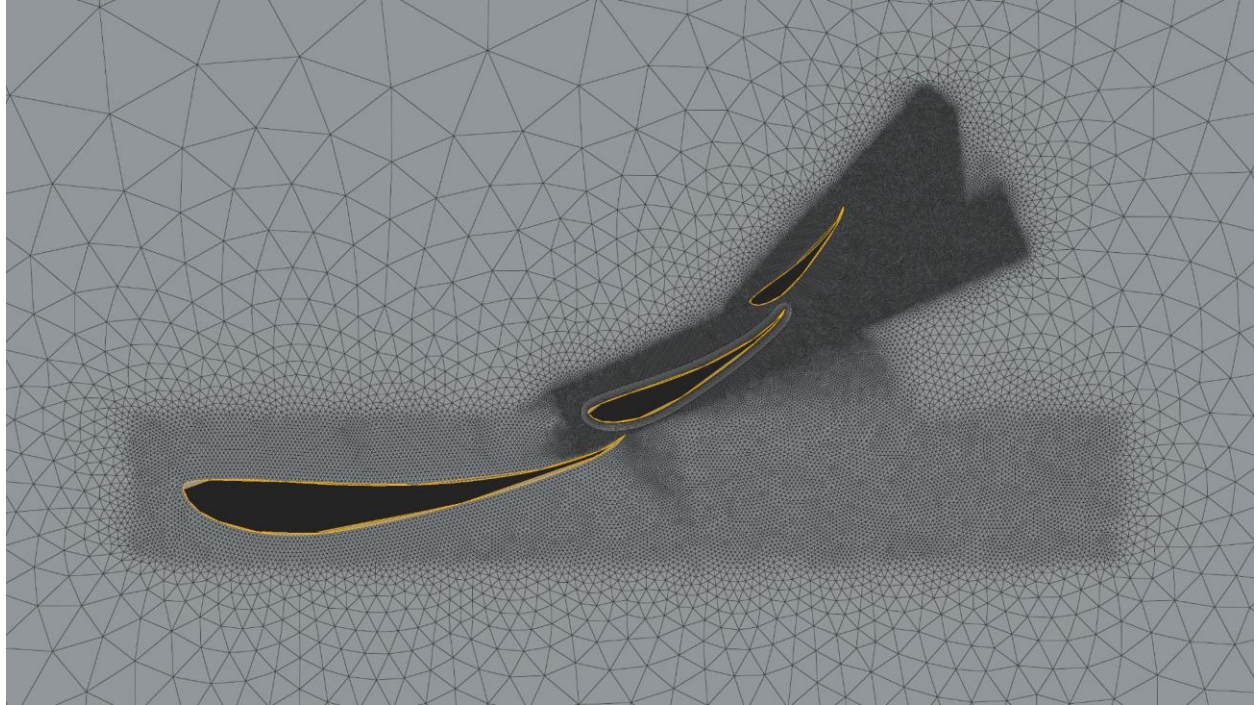
Section 3, Figure 1: Pre-meshing refinement zone Set-up

Next, a rectangular refinement zone was defined around each region of interest with an average element size of $C_{1,2,3}/128$. This aligns with the average size of the mesh elements in the surrounding refinement zone to ensure that the edge mesh element size transitions smoothly, which is critical for maintaining accuracy, stability, and convergence in the solution.

The center of the rectangular refinement zone was aligned with the tip of the trailing edge of each airfoil, such that the bulk of the refined mesh was up and to the right of the airfoil. The angle of

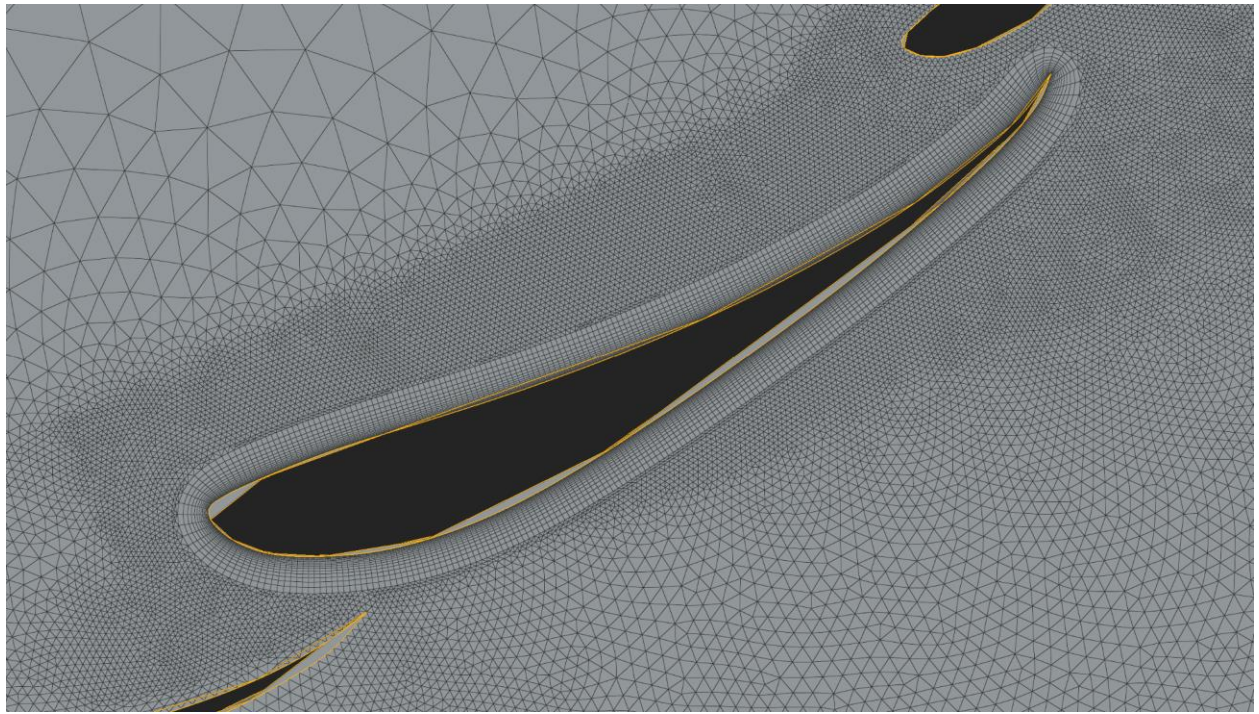
the refinement zones also align with the angle of each airfoil, as this would be the primary area of interest for our air flow.

The size of the aforementioned rectangular surface refinement zones was set to $2.2*C_{1,2,3}$ along the chord length, $0.3*C_1$ deep, and $0.3*C_{1,2,3}$ in the direction of thickness for the airfoils.

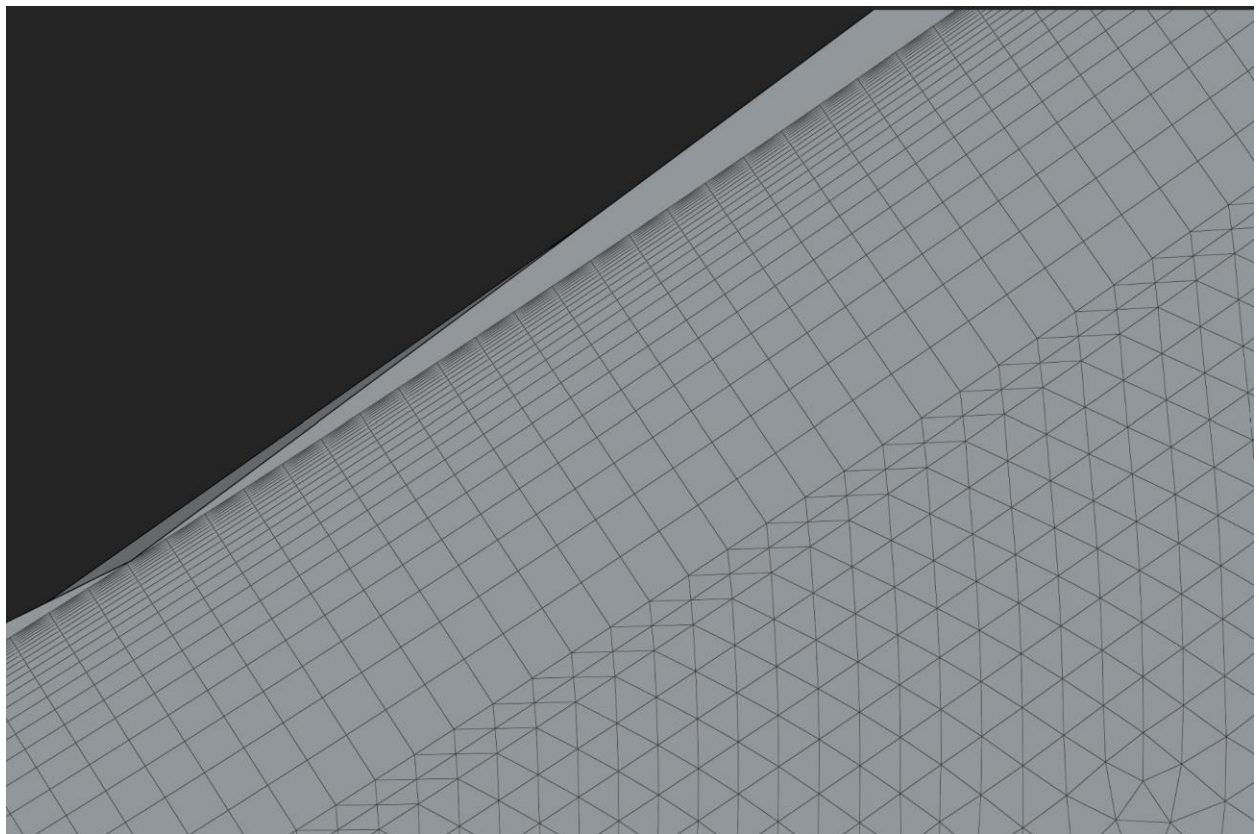


Section 3, Figure 2: Mesh Mid-distance View

Following surface meshing with a max element size set to C_1 , we set up the extrusion mesh. The element size along the extrusion direction was set to $C_1/10$. This mesh utilized quadrilateral elements, with two elements in depth to ensure accurate resolution in the boundary layer. The total volume mesh was then refined with the maximum element size set to $C_1 = 0.35$, ensuring sufficient – but not unnecessarily computationally expensive – resolution throughout. Our main area of interest was set on the middle airfoil for the refined edge layer to save on computational power and time.



Section 3, Figure 3: Middle Airfoil Meshed Rectangular Refinement Zone



Section 3, Figure 4: Close-up Edge Layer Mesh

Finally, the volume was meshed, with a prescribed maximum element size of C_1 , the original chord length. The meshing operation yielded a mesh with the following mesh statistics:

Type	Count
1 Nodes	1273137
2 Surface mesh elements	1679956
3 Volume mesh elements	1674360
4 Triangles	1656792
5 Quadrilaterals	23164
6 Tetrahedral elements	0
7 Hexahedral elements	17568
8 Pyramid elements	0
9 Prism elements	1656792

Section 3, Table 1: Mesh Quality Report

Section 4: Other Details

A key far-field setting was altered from its default by switching from “internal” to “external” turbulence flow type. This better matched the nature of the simulation and improved convergence.

Parallel processing was enabled using Intel MPI with 6 cores. In hindsight, using 4 cores may have been more efficient, but the turbulence simulation converged successfully—an improvement over the midterm.

The run was steady-state only. Consequently, no steady-to-unsteady transition was used. Default solver tolerances were kept; no custom convergence criteria were applied.

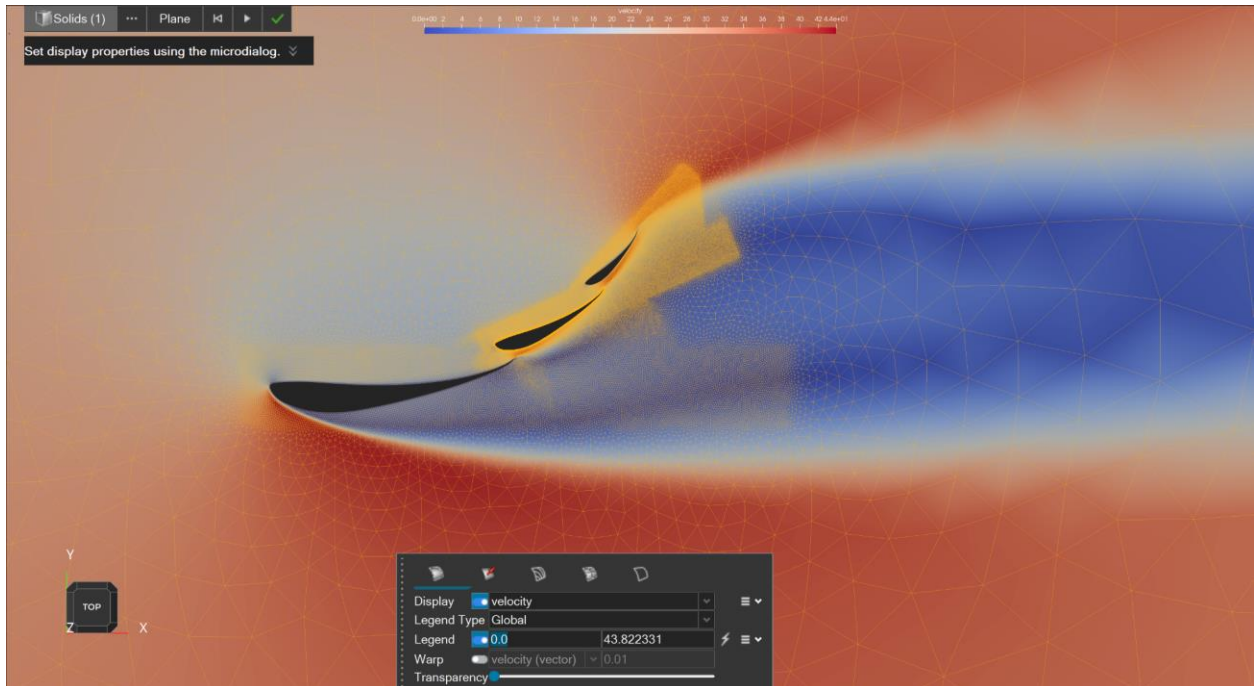
We did not use a formal mesh refinement study. Each group member created their own mesh with the same goals for redundancy purposes. As a result, only minor variation between them (i.e. the precise location of the refinement zones and the exact number of mesh elements). However, only one mesh was used for the final simulation.

There was room for further optimization. With better targeting of refinement zones, especially in low-gradient and far-field areas, the mesh size could have been reduced by an estimated 40% without loss of accuracy. Due to software issues on the user-end, no additional mesh iterations were created after the first run yielded satisfactory results.

Section 5: Results

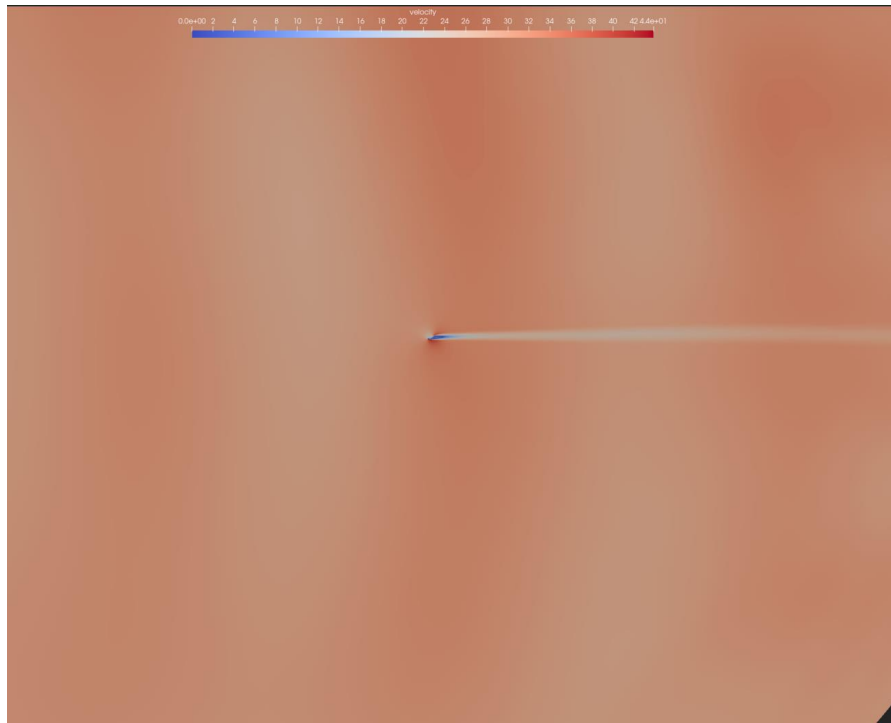
Total elapsed runtime ≈ 11.3 hours on Intel® Core i7-11800 CPU @ 2.30 GHz

6 cores utilized.

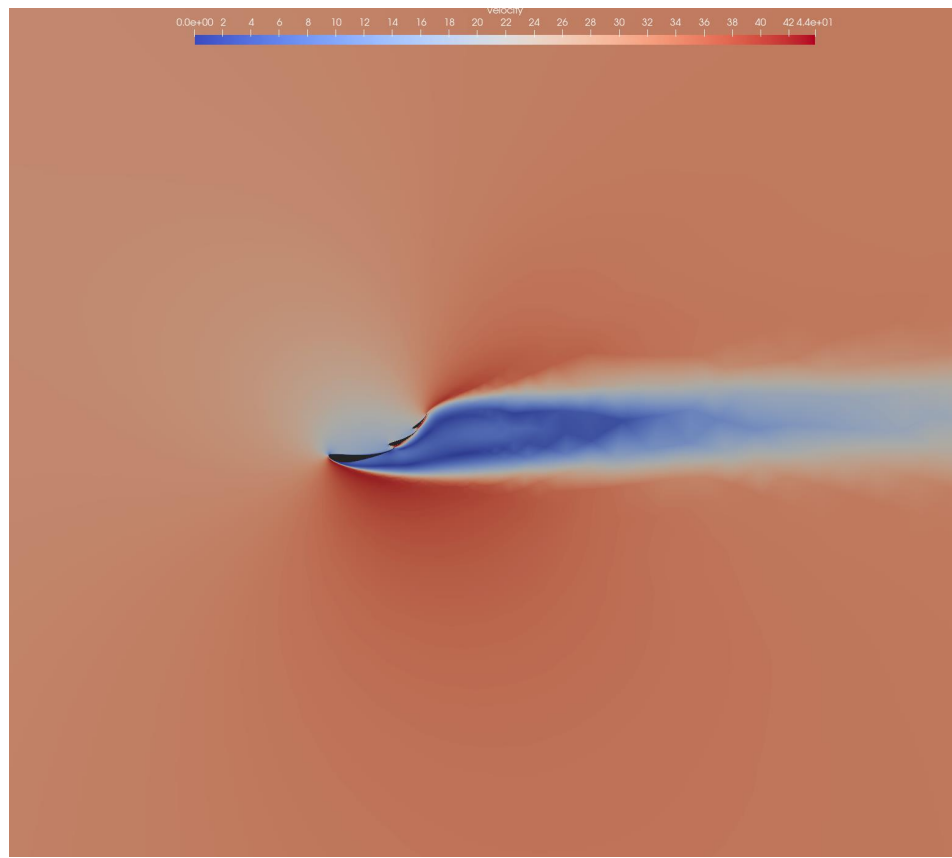


Section 5, Figure 1: Results of simulation overlaid on mesh

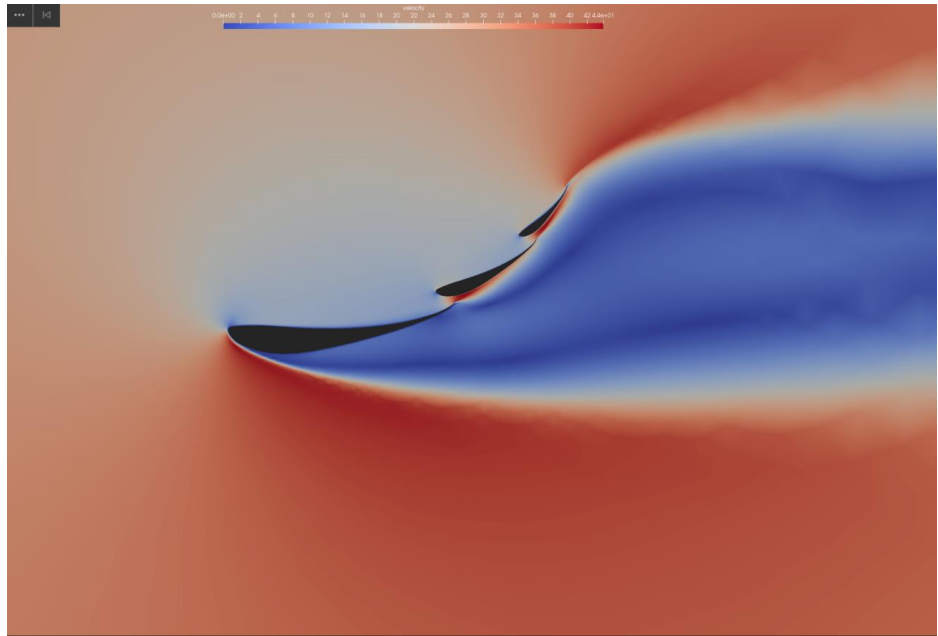
The figure above demonstrates that the mesh refinement used in this simulation was sufficient. The boundary region and wake is large and consistent with expectations for this airfoil. Overall, sufficient mesh resolution and consistency between the boundary layer and volume meshes.



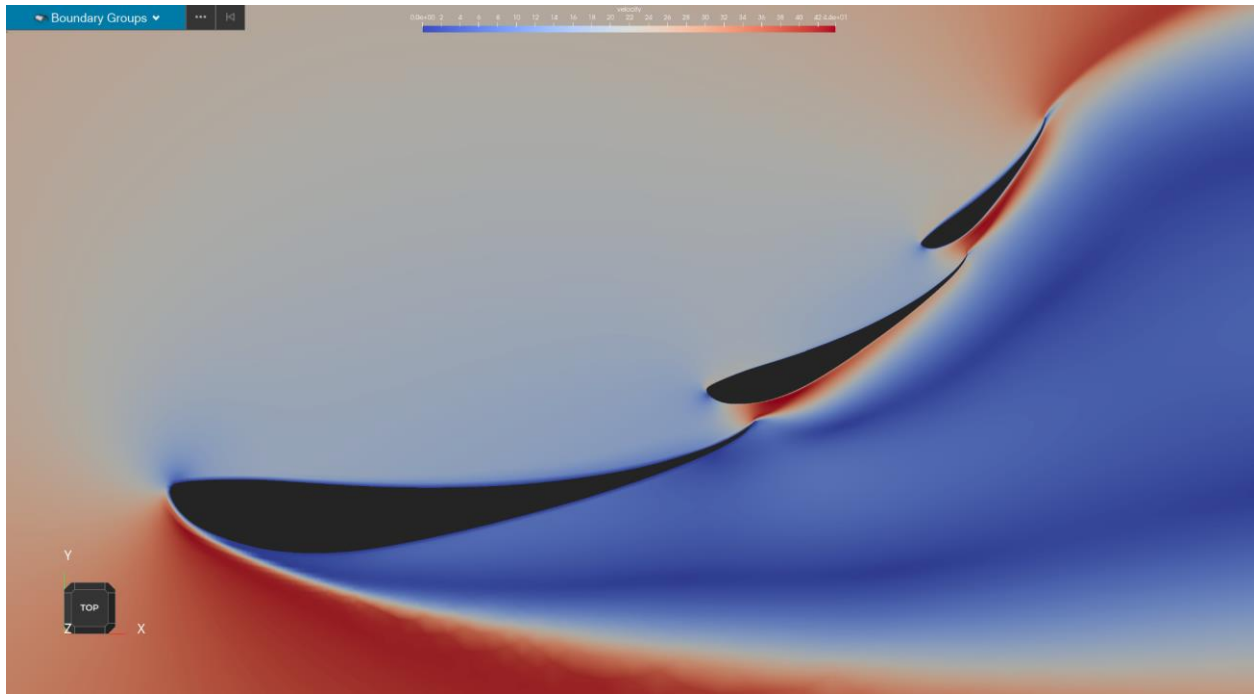
Section 5, Figure 2: full-view velocity (m/s)



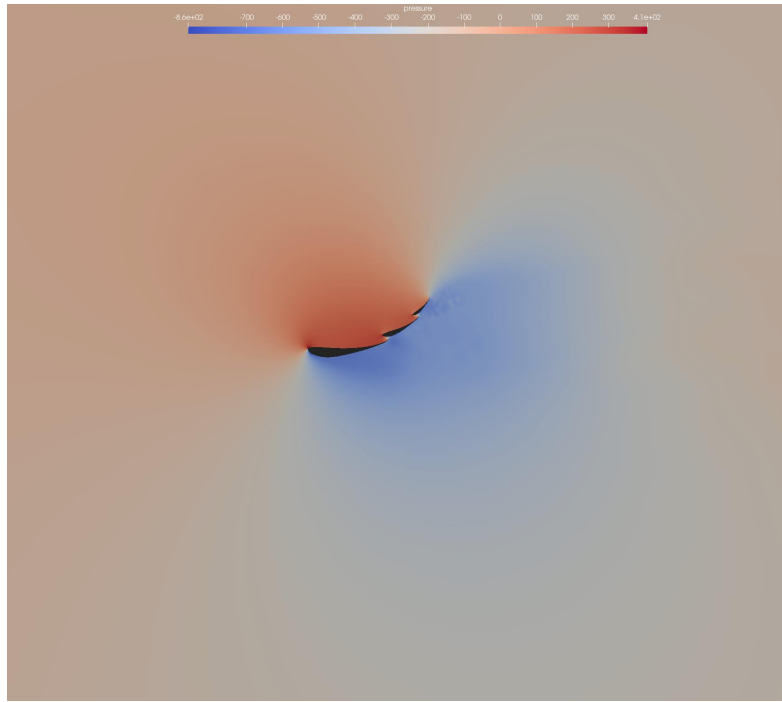
Section 5, Figure 3: Mid-view velocity (m/s)



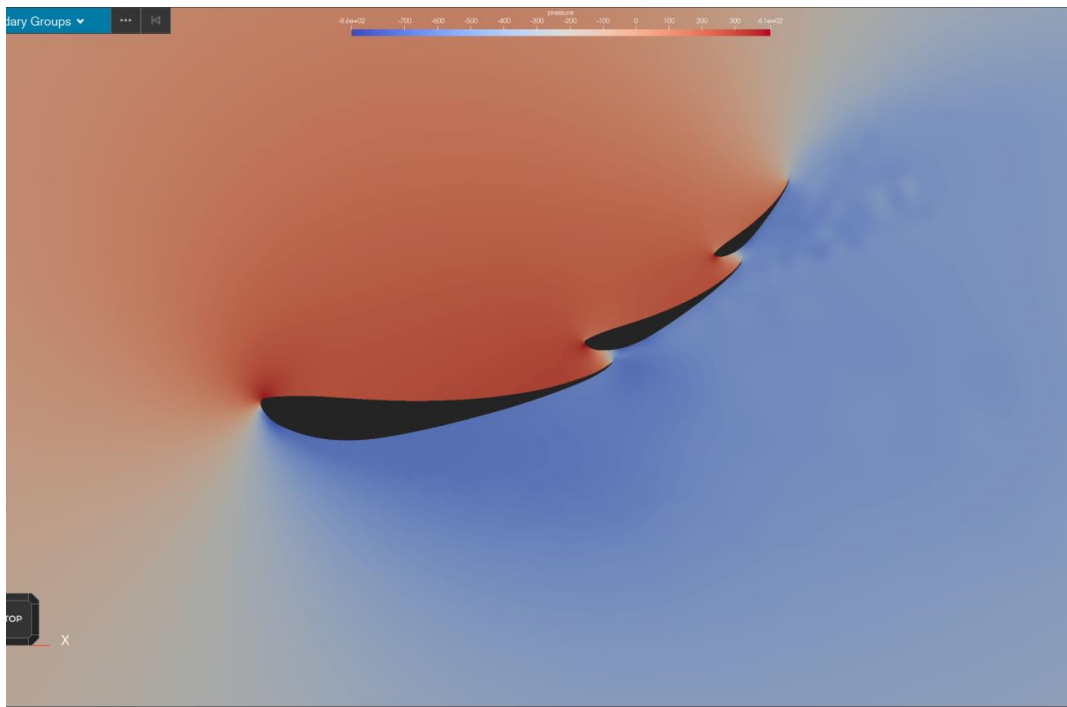
Section 5, Figure 4: Close-view velocity (m/s)



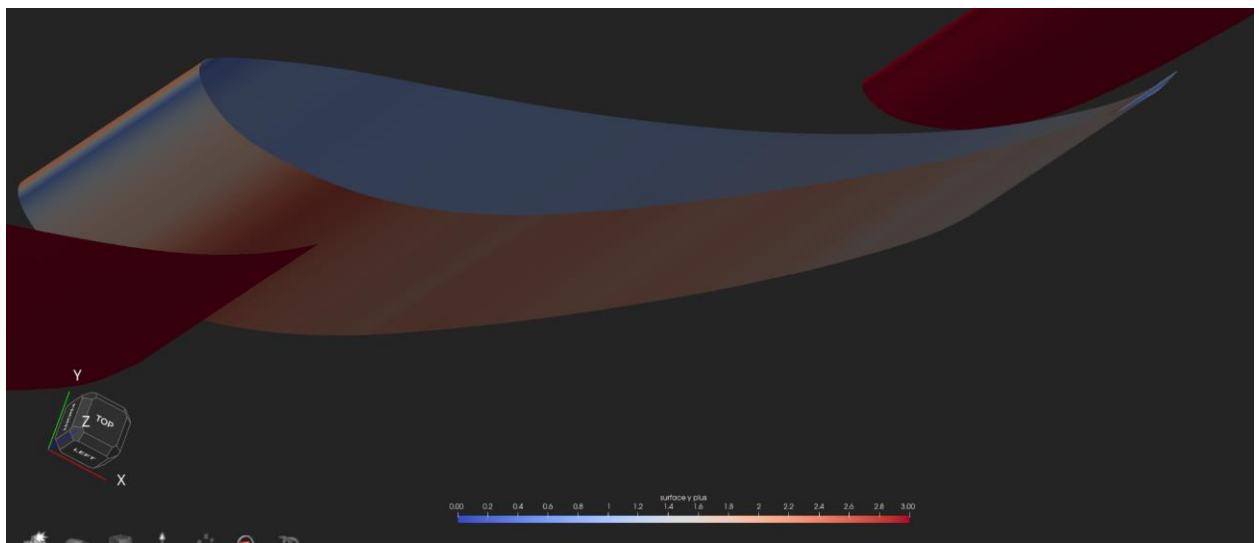
Section 5, Figure 5: Super Close-view velocity (m/s)



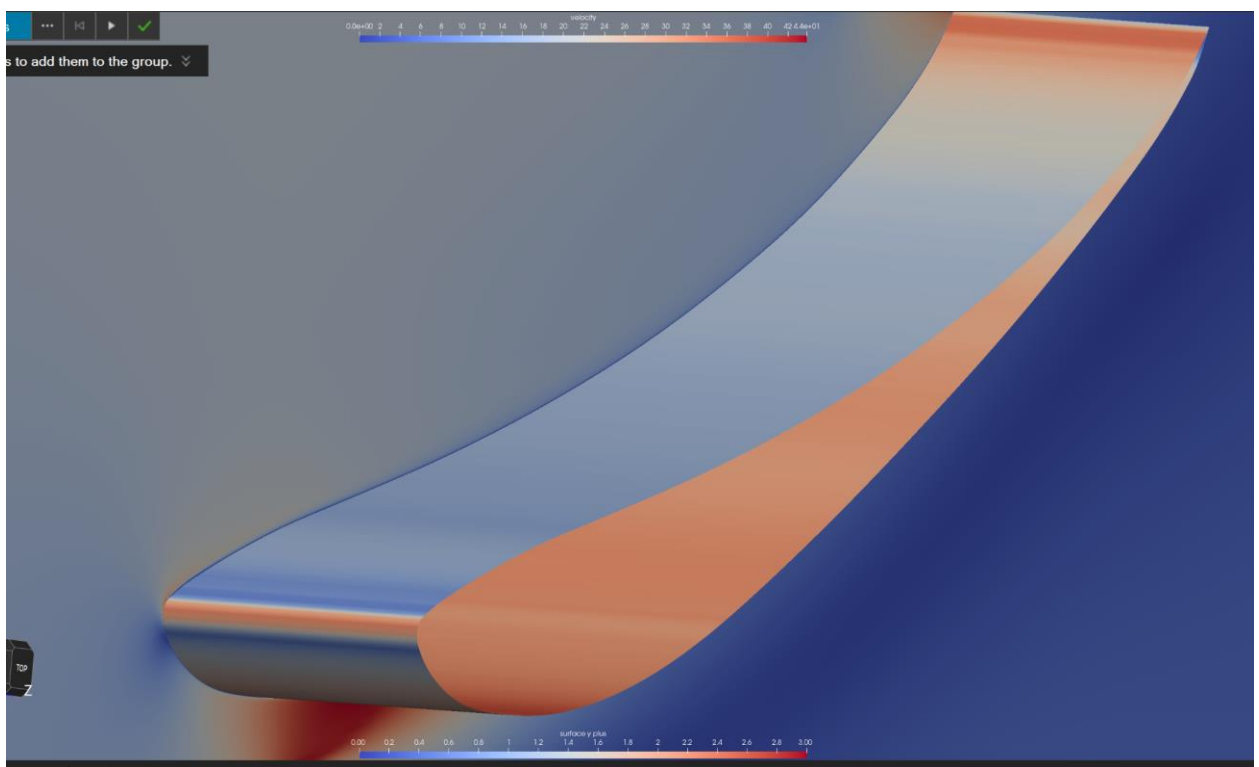
Section 5, Figure 6: Full-View Pressure field



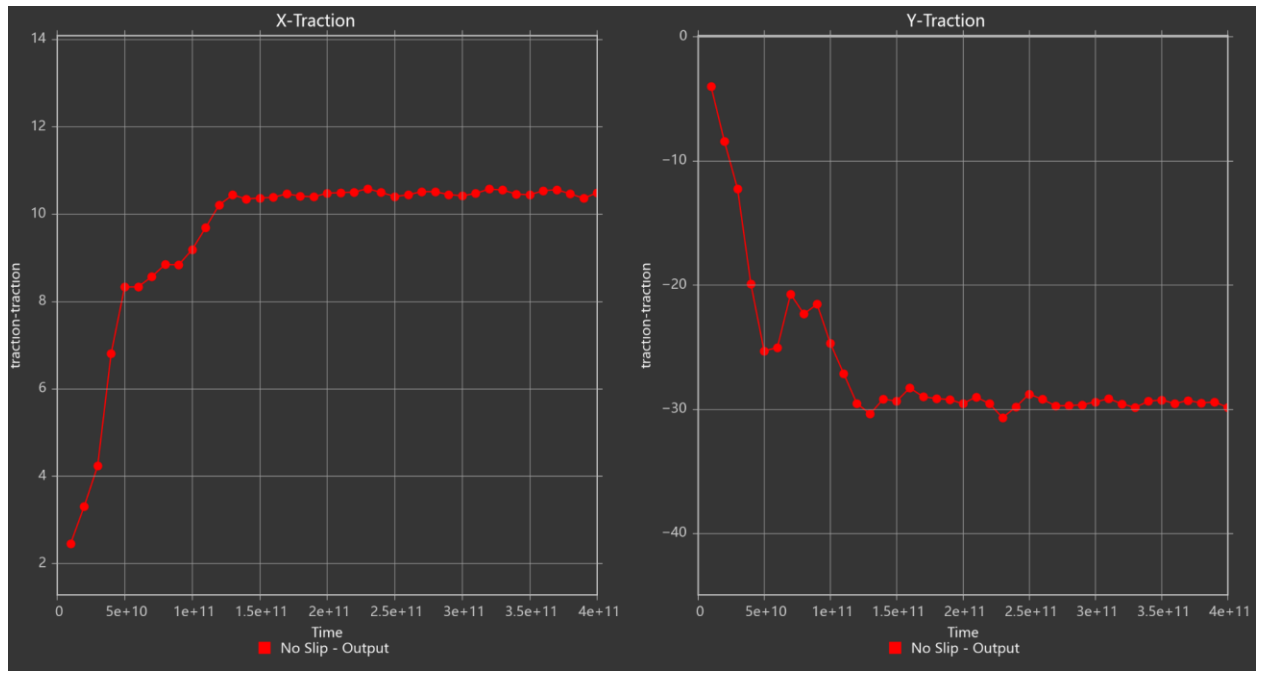
Section 5, Figure 7: Close-View Pressure field



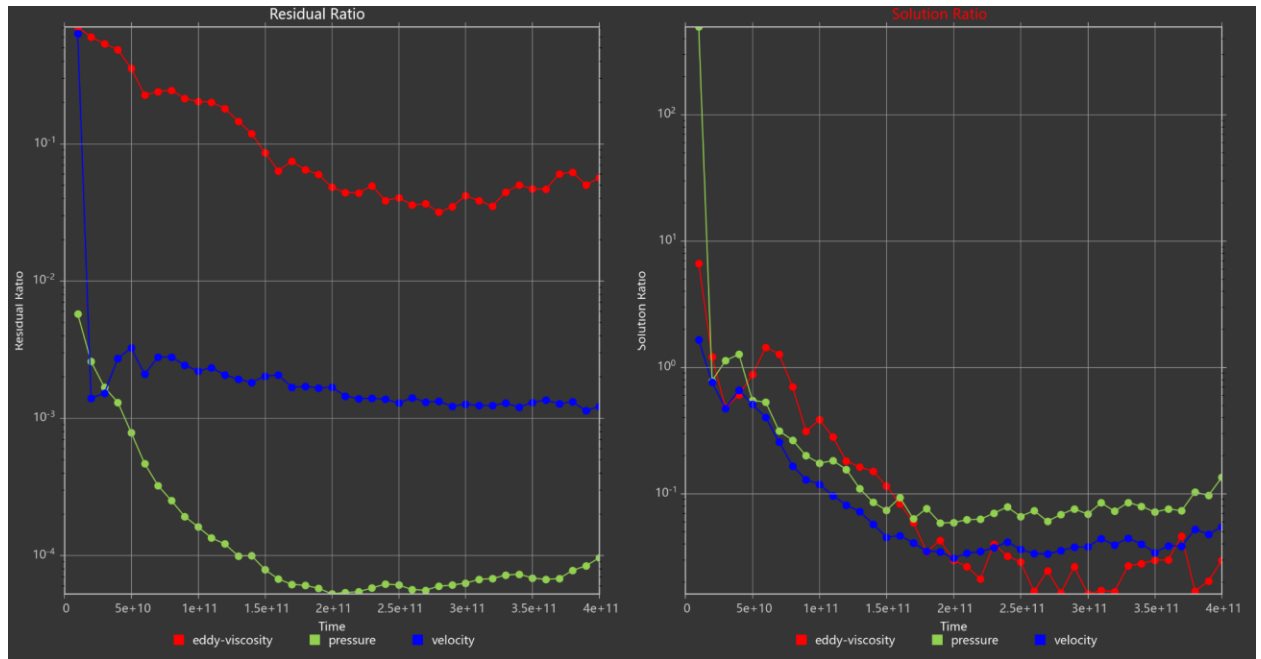
Section 5, Figure 8: Surface y -plus. Surface y -plus reaching maximum value of 2.8.



Section 5, Figure 9: Mid-airfoil Surface y -plus top view.



Section 5, Figure 10: Traction X & Y-component graphs.



Section 5, Figure 11: Residual & Solution ratio.

The lift and drag coefficients can be calculated using the following equations, simply using the ultimate values calculated at the end of the simulation runtime:

$$C_D = \frac{D}{\left(\frac{l}{2}\right) \rho U_\infty^2 b c} \quad C_L = \frac{L}{\left(\frac{l}{2}\right) \rho U_\infty^2 b c}$$

where $b = 0.07\text{m}$, and $c = 0.56\text{ m}$ the total chord length.

With L being the y-component in the Lift graph and D being the x-component in the Drag graph we get:

$$\begin{aligned} C_D &= \frac{10.2}{\left(\frac{l}{2}\right) * (1.127 \text{ kg/m}^3) * (30 \text{ m/s})^2 * 0.07 * 0.56} & C_L \\ &= \frac{-29.5}{\left(\frac{l}{2}\right) * (1.127 \text{ kg/m}^3) * (30 \text{ m/s})^2 * 0.07 * 0.156} \\ C_D &= 0.513 & C_L &= -1.484 \end{aligned}$$

Section 6: Closing remarks

The CFD simulation of the S1223 airfoil produced a converged and meaningful solution, and the results align with expectations for a high camber, inverted airfoil designed for downforce. Our results yielded a lift coefficient of 1.484 which is only slightly larger than what was seen graphically in section 1 from the referenced *Multi Element Wing Analysis*. The slight deviation can be attributed to the variation in angles of attack between airfoils. Our results yielded a high drag coefficient of 0.531 which can be easily justified by observing the chosen geometry. The high angles of attack for each stacked airfoil increase the total bluff body surface area interacting with the flow, drastically increasing the drag force and coefficient. The total resulting downforce was approximately 30 N which also falls within the reasonable bounds of lift forces for airfoils.

Moreover, the outcomes of our simulation match expectations for our stacked-inverted airfoil with a strong low-pressure region beneath and to the right of the leading edge indicates accelerated airflow and confirms the creation of negative lift (downforce). This low-pressure zone shows that the geometry and by extension the car is being pulled downward.

The final simulation achieved a maximum surface y -plus value of approximately 2.4, which is within an acceptable range for accurate turbulence modeling using wall-resolved approaches—ideally, values near or below 1 are preferred for high-fidelity results. To further validate the quality of our solution, we examined the gaps between the stacked airfoils—regions of complex flow behavior where quickly-varying velocity gradients were observed. In these areas, the principle of mass conservation was satisfied, as the product of local velocity and channel height remained consistent across streamlines. This further lent itself to corroborating the credibility to the solution accuracy in regions of high shear.

One noteworthy feature observed in the simulation is the formation of a free shear layer at the trailing edges of the airfoils, especially within the gaps between elements. This region is marked by a sharp velocity gradient between fast-moving flow and adjacent slower or recirculating regions, indicating strong shear and potential vortex shedding. Such behavior is typical in high-lift aerodynamic configurations and suggests enhanced flow mixing and momentum exchange. While a detailed analysis of vortex dynamics was beyond the scope of this report, the presence of these shear layers aligns with the expected aerodynamic behavior.

Earlier in the project, we encountered issues with convergence, particularly when attempting to simulate convergence. For the midterm project, we were unable to identify the source of the issues. However, we continued our investigation and ultimately traced our issues back to mesh and boundary condition errors, specifically the omission of a slip condition at certain interfaces. These were resolved in the final mesh. Additionally, we corrected an important far-field setting by switching from the default “internal” to “external” turbulence flow type, which better reflects the nature of our simulation. Furthermore, we improved our computational speed by enabling parallel

processing using Intel MPI with 6 cores. Although we later learned that using 4 out of the 6 available cores would have been more optimal, the turbulent simulation converged—marking a substantial improvement from the midterm project.

In retrospect, there was significant potential to reduce the mesh size by approximately 40% through better refinement zone targeting. We recognized that areas with minimal variation in the solution, as well as areas far outside the area of interest, could have been meshed more coarsely without compromising accuracy, had we been able to generate additional mesh iterations. Unfortunately, technical limitations and software usability issues prevented us from exploring this further.

While this concludes the project, if we had more time, we would continue exploring this problem by investigating unsteady flow effects to capture transient behaviors such as vortex shedding and wake interaction between elements. Additionally, we would alter the geometry to include supporting struts and perhaps some boundary conditions below the airfoil to better capture ground effect and the full aerodynamic interaction with the rest of the car.

Ultimately, this project proved to be a highly valuable educational experience. From a pedagogical perspective, there was great value in all the setbacks we encountered, even the frustrating ones. We gained practical insights into CFD simulation workflows, meshing strategies, and solver configuration. Our analysis, which focused primarily on the second (middle) airfoil, targeted an under-researched area of aerospace engineering. The results obtained were consistent with expectations and served as a meaningful demonstration of the principles learned throughout the course.

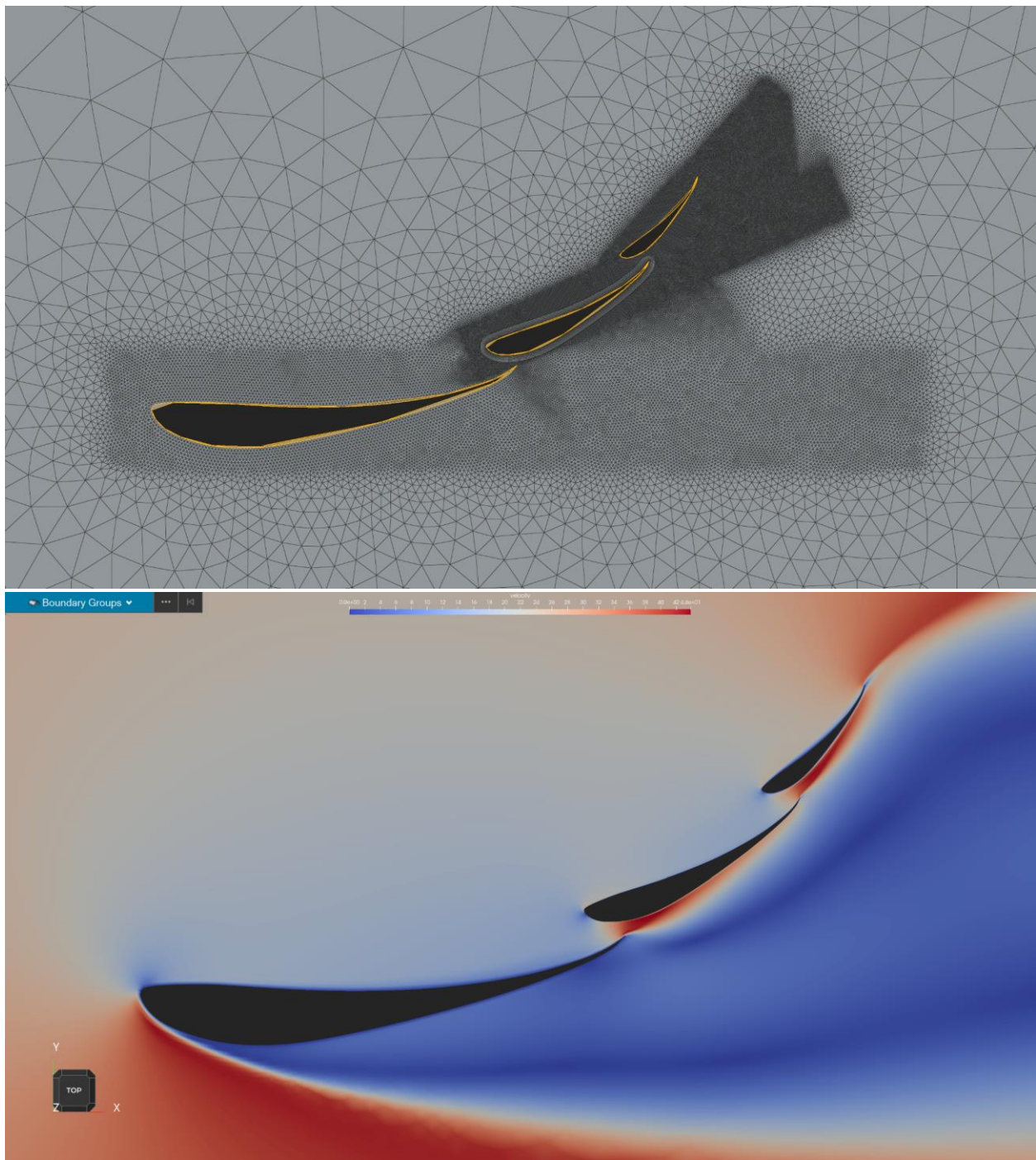
Section 7: Appendix

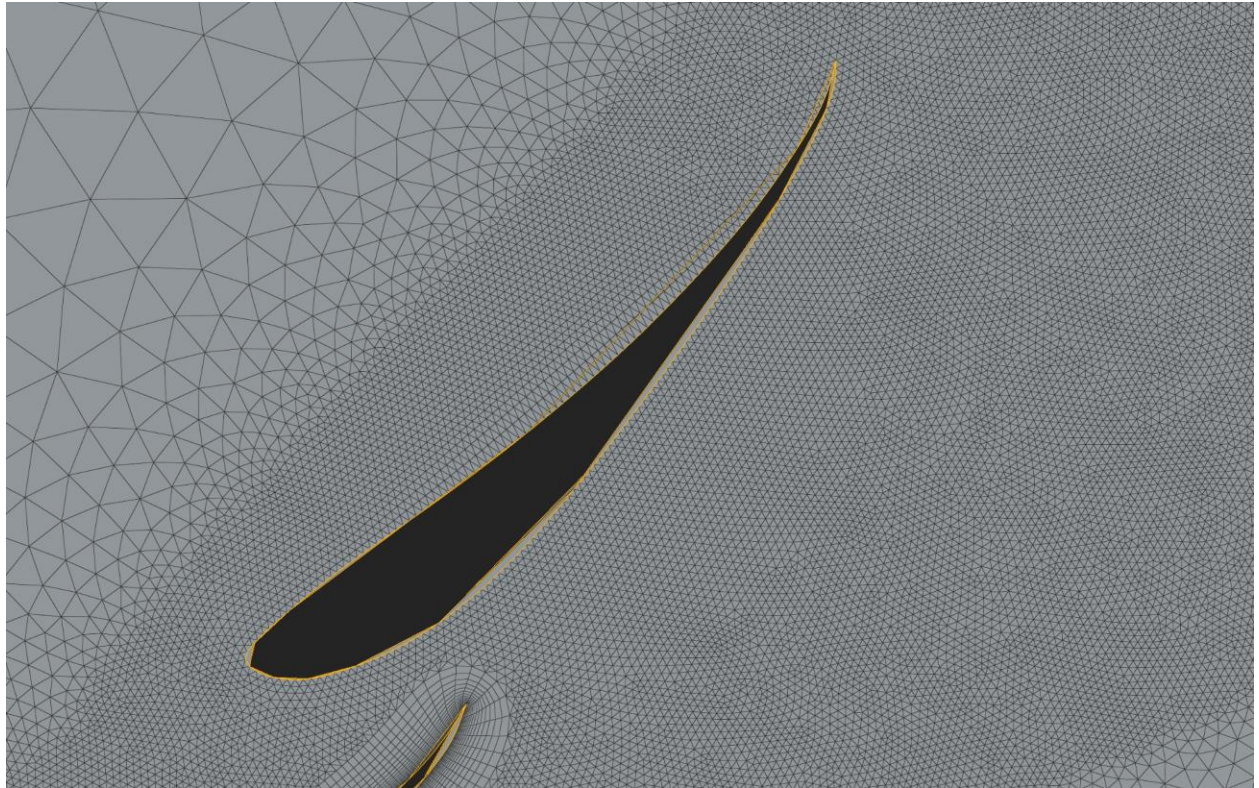
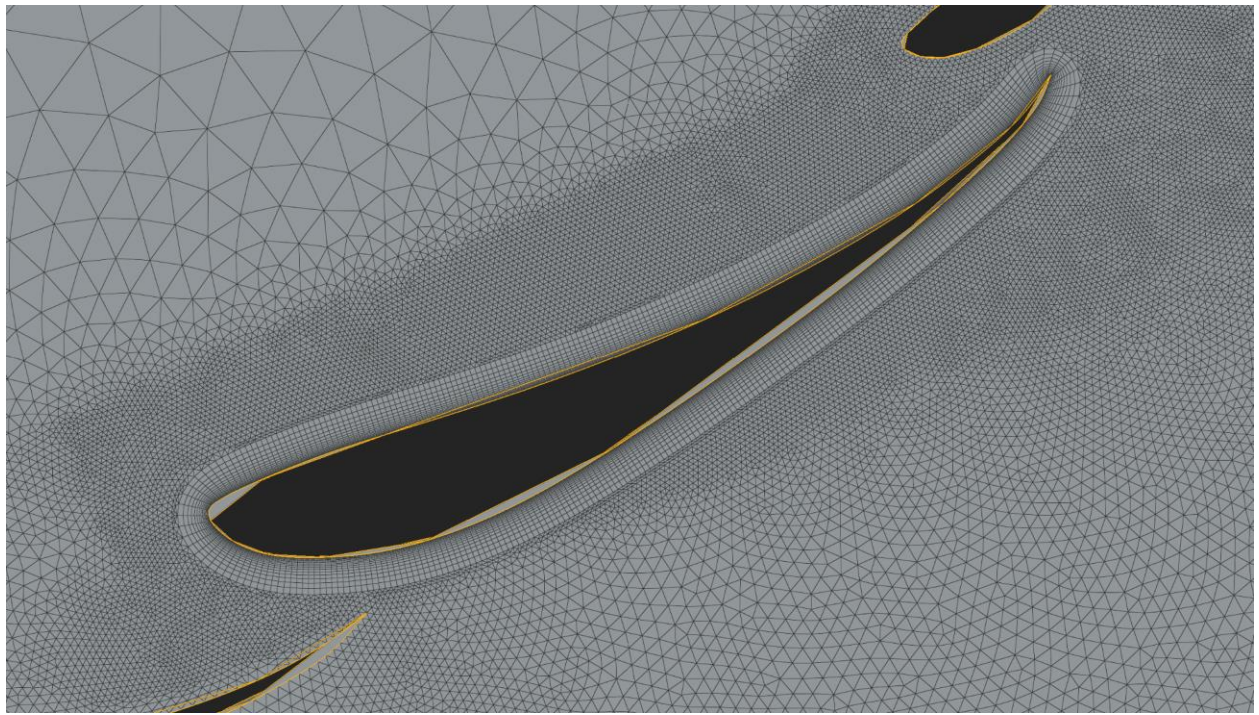
Resources:

1. Occam's Racers. (2023, August 16). *DIY Selig S1223 wing*. Retrieved from <https://occamsracers.com/2023/08/16/diy-selig-s1223-wing/>
2. Benzing, E. (n.d.). *Profilo software for airfoils*. Retrieved from <http://www.benzing.it/enrico.profilo.htm>
3. Airfoil Tools. (n.d.). *S1223 airfoil details*. Retrieved from <http://airfoiltools.com/airfoil/details?airfoil=s1223-il>
4. Arabi, M. A., & Inam, M. I. (n.d.). *Aerodynamic characteristics of an FSAE car rear wing with multi-element S1223 airfoil*. SSRN. Retrieved from <https://www.ssrn.com/>
5. Altair Community. (n.d.). *How do I determine drag force, downforce, drag coefficient, and lift coefficient from CFD analysis in HyperWorks CFD?* Retrieved from <https://community.altair.com/discussion/21027/how-i-know-drag-force-downforce-drag-coefficient-and-lift-coefficient-from-cfd-analysis-in-hyperworks-cfd>
6. Engineers Edge. (n.d.). *Viscosity of air, dynamic and kinematic*. Retrieved from https://www.engineersedge.com/physics/viscosity_of_air_dynamic_and_kinematic_14483.htm
7. Ambhore, P. J., & Mali, S. (2016). *Multi Element Wing Analysis*. IOSR Journal of Mechanical and Civil Engineering, 13(2 Ver. I), 95–100. <https://doi.org/10.9790/1684-13020195100>

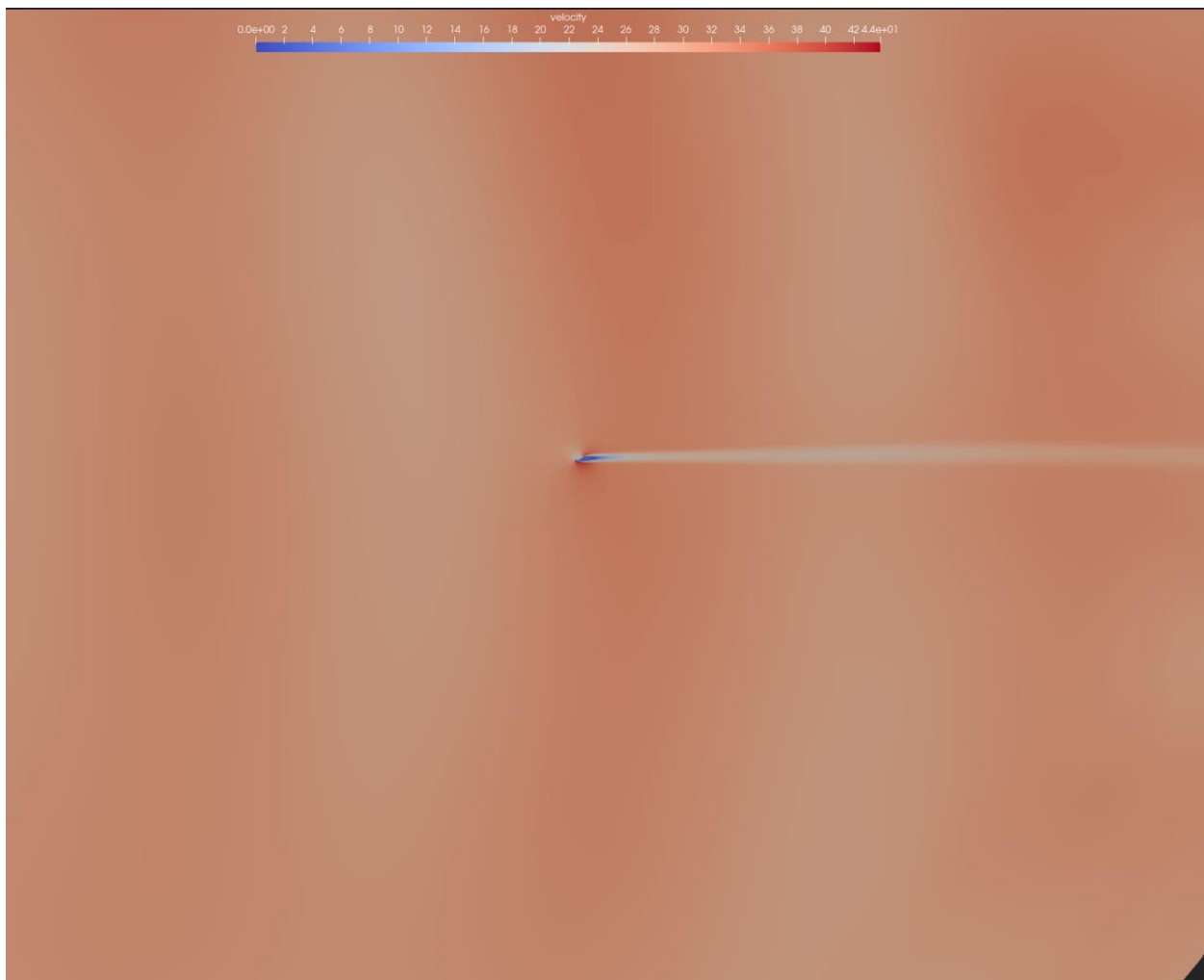
Final Images

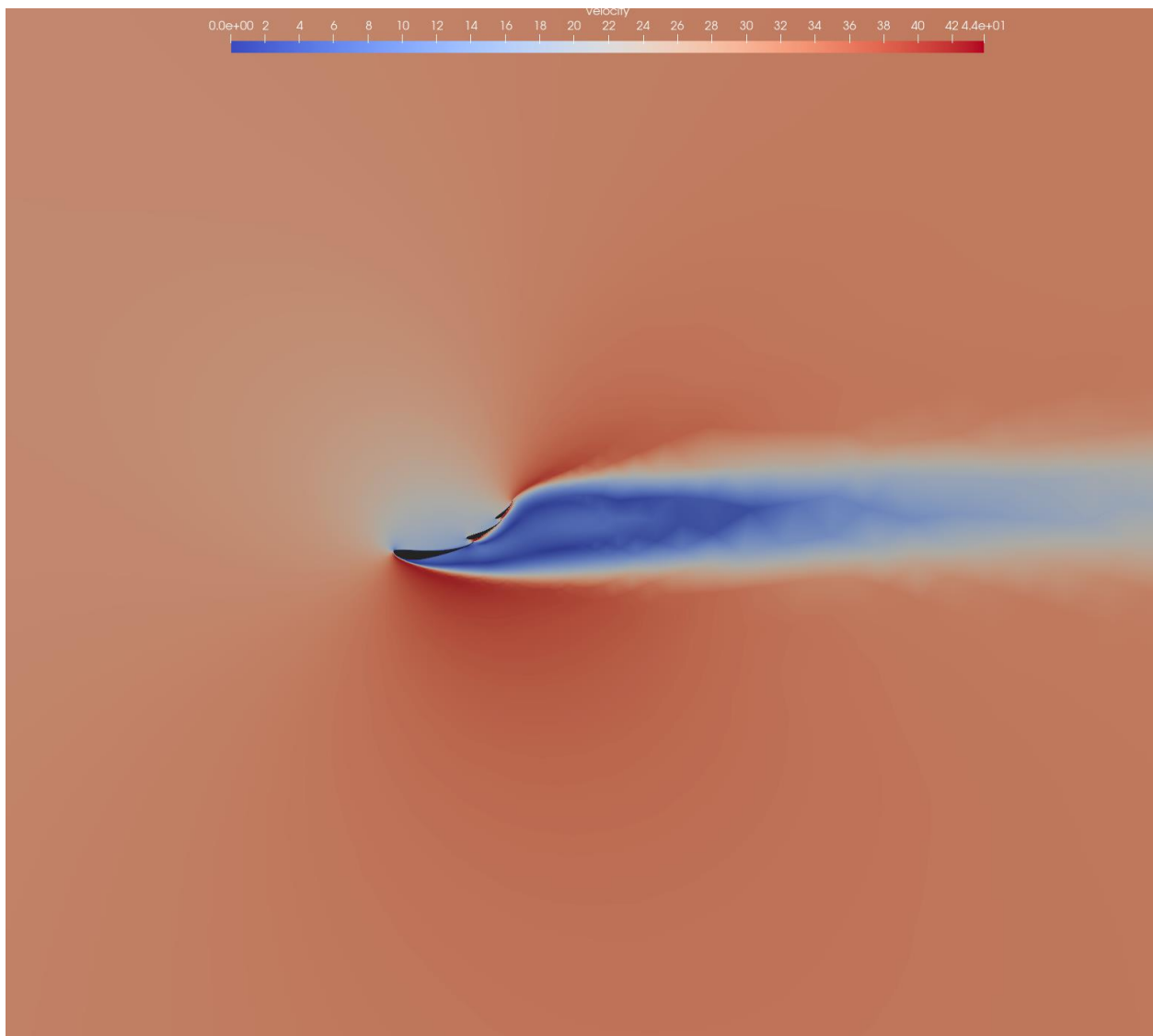


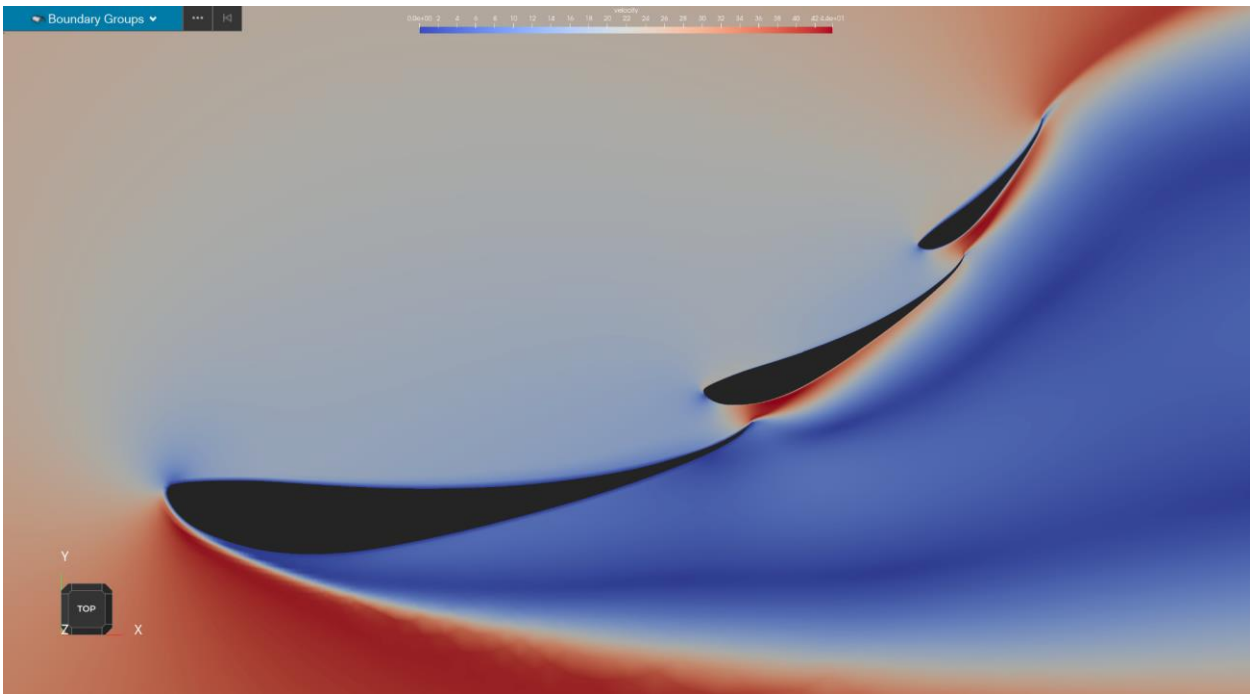
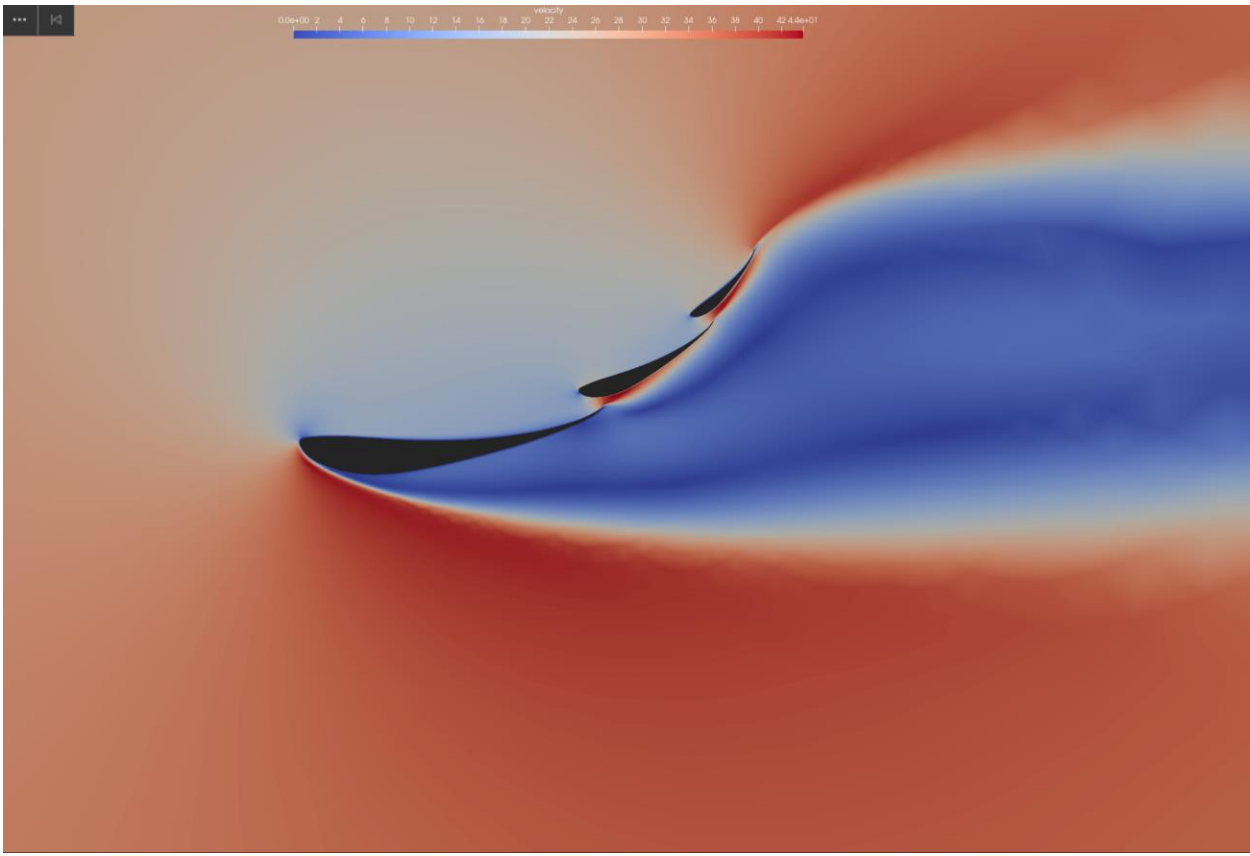




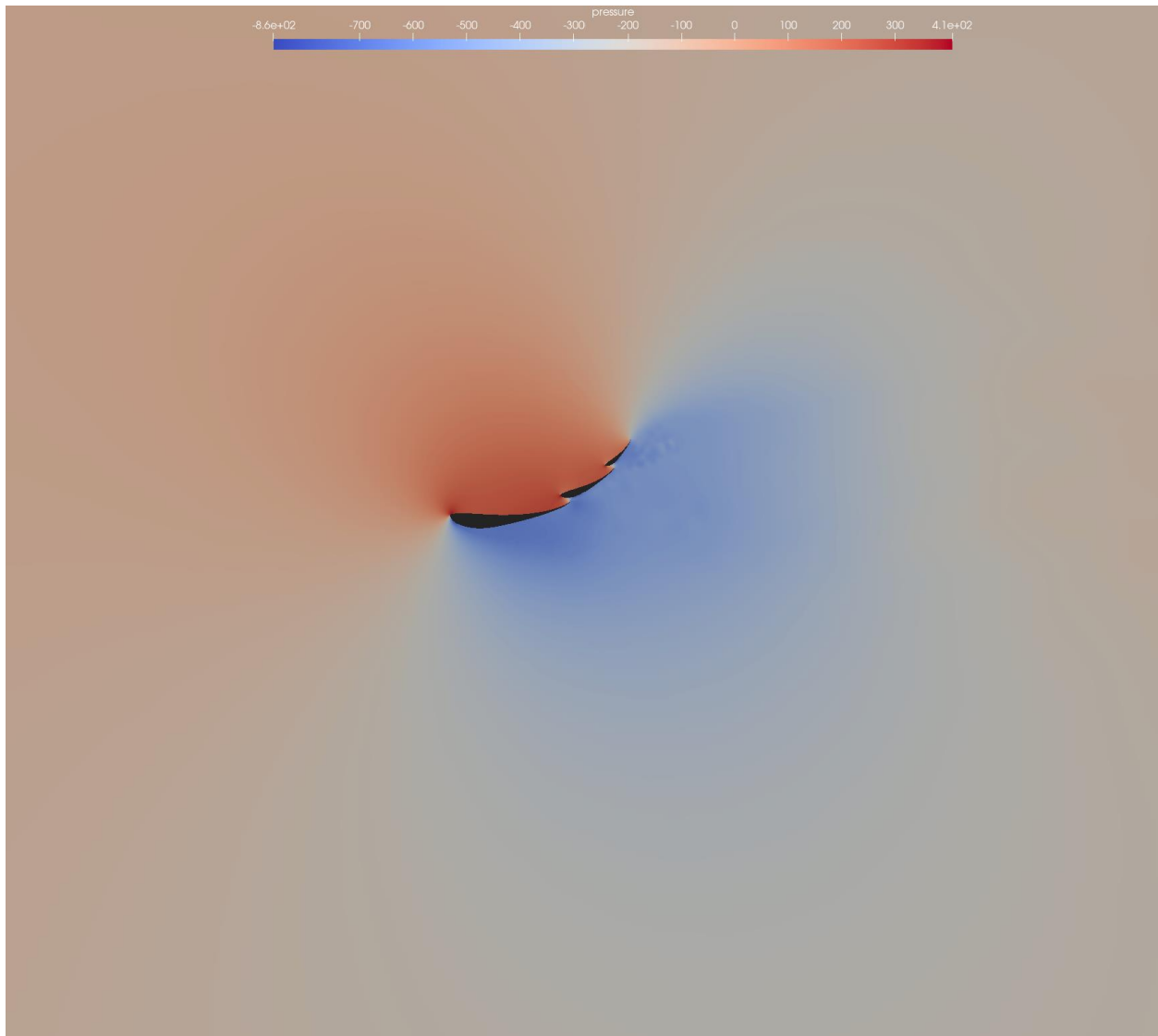
Type	Count
1 Nodes	1273137
2 Surface mesh elements	1679956
3 Volume mesh elements	1674360
4 Triangles	1656792
5 Quadrilaterals	23164
6 Tetrahedral elements	0
7 Hexahedral elements	17568
8 Pyramid elements	0
9 Prism elements	1656792

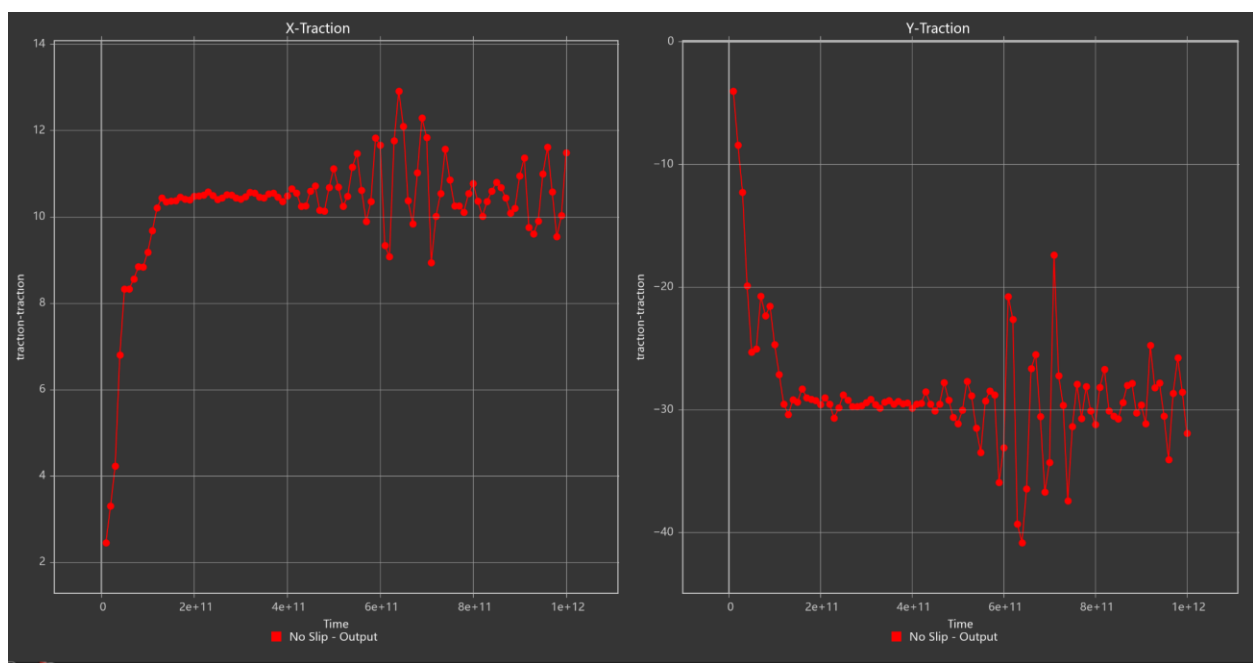
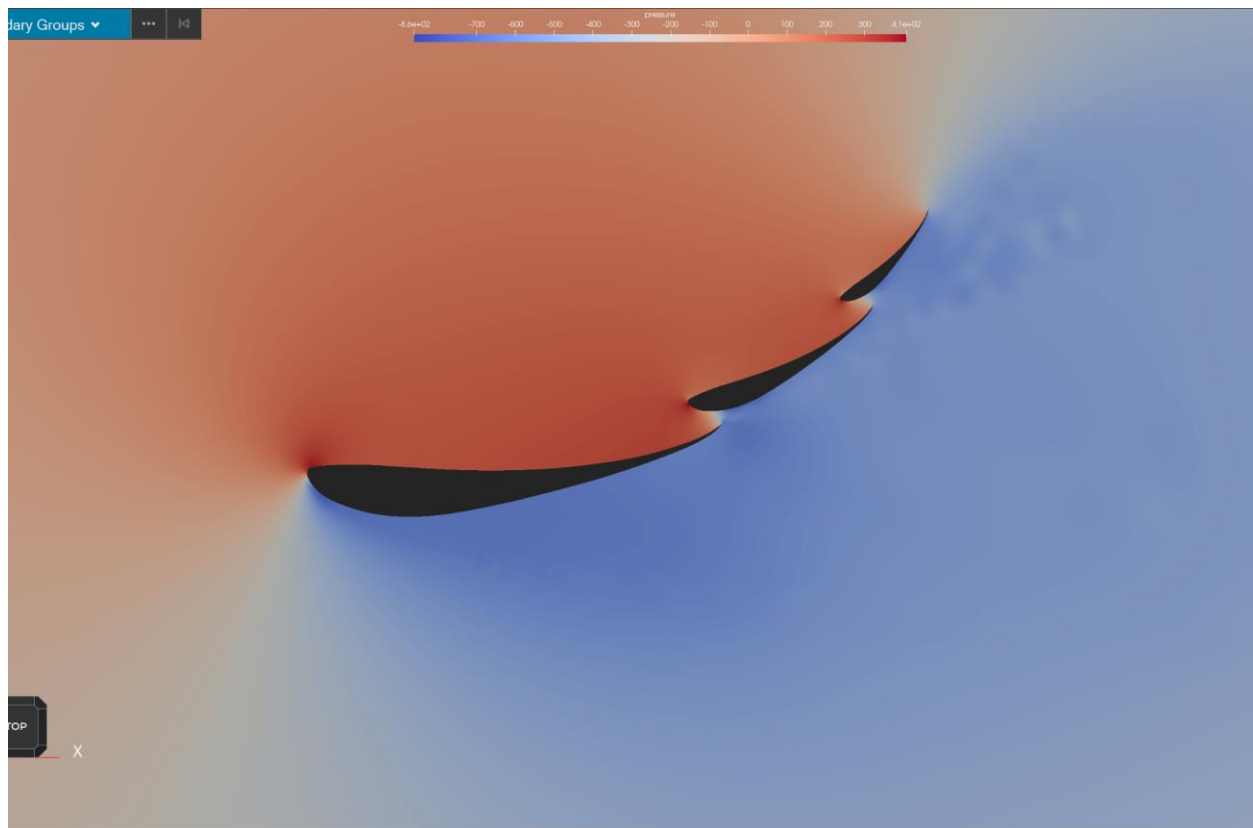


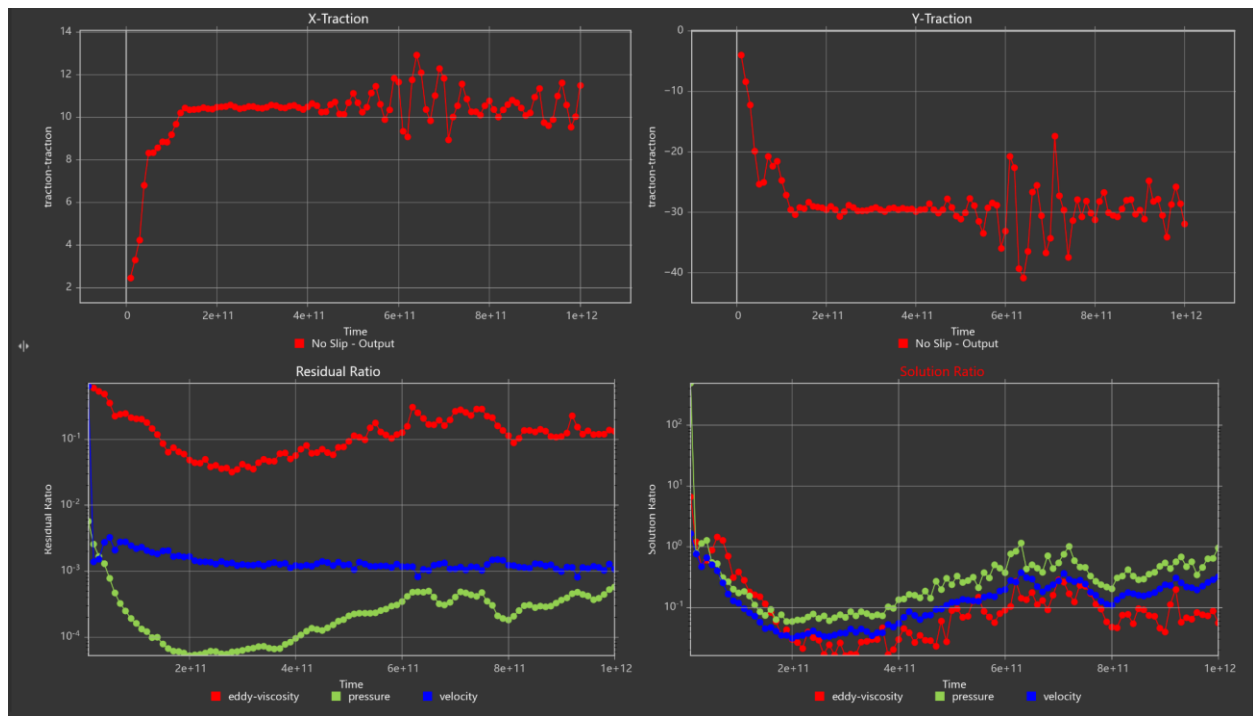


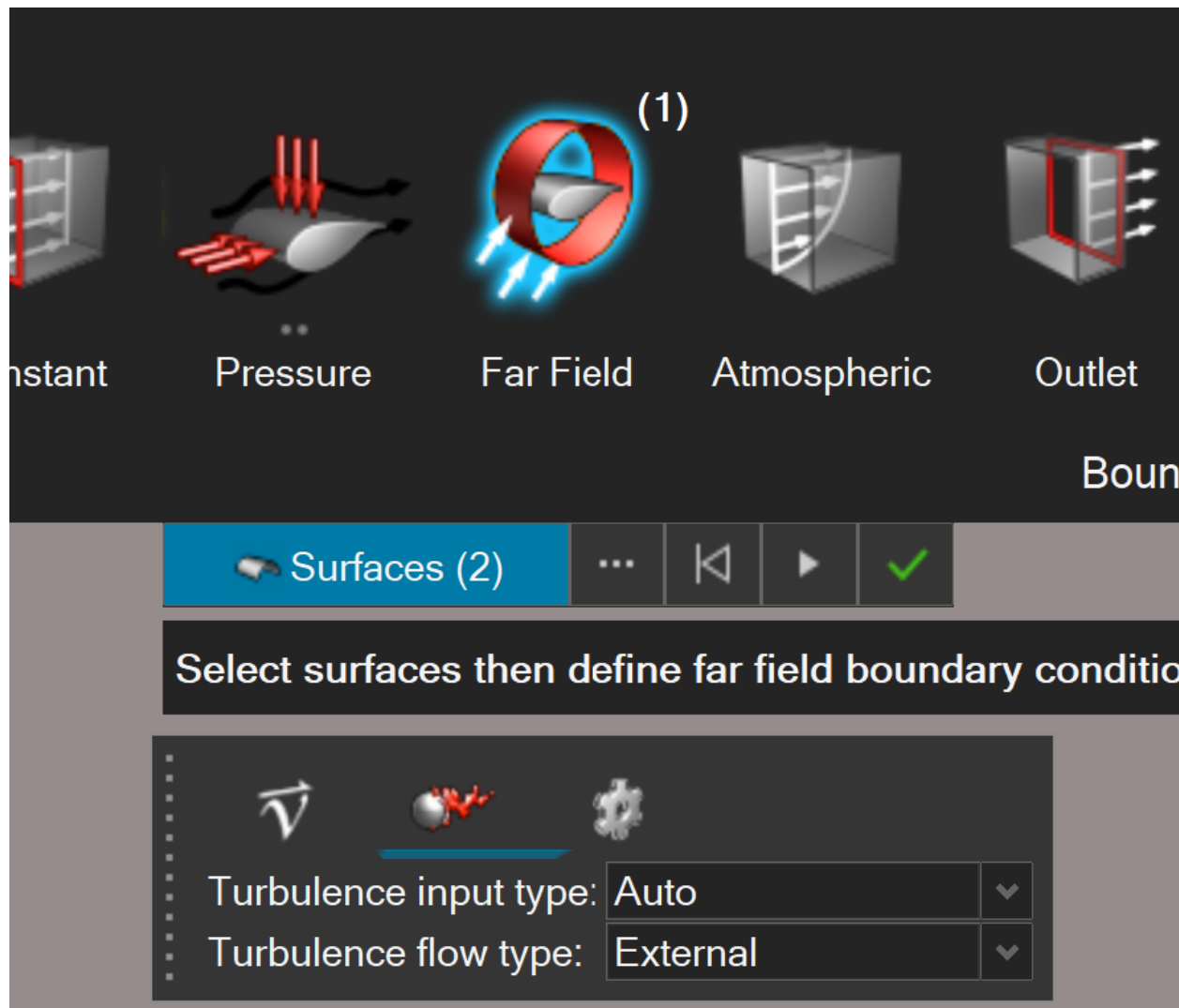


PRESSURE









Launch AcuSolve

Run definition 

Problem name: stacked_foil_sim

Problem directory: C:\hnic Institute\Documents\CFD\Project\final  

AcuRun path: \cfdsolvers\acusolve\win64\bin\acuRun.bat 

Additional arguments:

Processes to run: all 

Parallel processing: Intel MPI 

Number of processors: 6

Use hybrid message passing

Number of threads: 1

Automatically define pressure reference

Default initial conditions 

Restart 

Planning

Teachers Comments:

This looks fine. I suggest to start with 2D or 3D segmented/slab geometry (e.g., a cross-section, a few cross-sections or a "thin" 3D slab), in the mid-term project.

Your team should look into two aspects at the earliest:

- 1) what is the target/goal for the mid-term project (and what will be possible for the final project building upon the mid-term project)
- 2) what are the immediate next steps for the mid-term project and which team member will do which ones (e.g., geometry, flow conditions including BCs, meshing, running analysis, post-processing, etc.)

Airfoil links:

- [Enrico Benzing - Profili](#)
- [Double Wing with Guerney Flap | 3D CAD Model Library | GrabCAD](#)

Airfoil decision:

S1223 - Selig S1223 high lift low Reynolds number airfoil

<http://airfoiltools.com/airfoil/details?airfoil=s1223-il>

[s1223 paper](#)



Proceedings of ICME 2023
14th International Conference on Mechanical Engineering
18-19 December 2023, BUET, Dhaka, Bangladesh



Aerodynamic Characteristics of an FSAE Car Rear Wing with Multi-Element S1223 Airfoil

Md. Almamun Arabi^{1,a)}, Mohammad Ilias Inam¹

¹Department of Mechanical Engineering, Khulna University of Engineering & Technology, Khulna-9203, Bangladesh

^{a)} Corresponding author: almamun05012@gmail.com

Set up:

- Chord length (c) = 350 mm = 0.35 m
- Air velocity: 90 m/s
- no-slip condition is applied to the airfoil's surface
 - No slip boundary condition on airfoil surface with "Wall velocity type" as "Zero" and "Near-wall treatment" set as "Wall Resolved"
- Slip applied to Circular planes of the large fairfield ircle
- "Symmetry: these are applied on side planes (front and back surfaces), and
- typically do not require any additional inputs past selecting the target surface"

- Air Properties¹:

- Density: 1.127 kg/m³
- Viscosity: 1.918e-5 kg/m/s

Properties of air at 1 atm pressure

Temp T, °C	Density Air ρ , kg/m ³	Specific Heat of Air c_p , J/kg-K	Thermal Conductivity Air k , W/m-K	Thermal Diffusivity Air α , m ² /s	Dynamic Viscosity Air μ , kg/m-s	Kinematic Viscosity Air ν , m ² /s	Prandtl Number Air Pr
-150	2.866	983	0.01171	4.158×10^{-6}	8.636×10^{-6}	3.013×10^{-6}	0.7246
-100	2.038	966	0.01582	8.036×10^{-6}	1.189×10^{-5}	5.837×10^{-6}	0.7263
-50	1.582	999	0.01979	1.252×10^{-5}	1.474×10^{-5}	9.319×10^{-6}	0.7440
-40	1.514	1002	0.02057	1.356×10^{-5}	1.527×10^{-5}	1.008×10^{-5}	0.7436
-30	1.451	1004	0.02134	1.465×10^{-5}	1.579×10^{-5}	1.087×10^{-5}	0.7425
-20	1.394	1005	0.02211	1.578×10^{-5}	1.630×10^{-5}	1.169×10^{-5}	0.7408
-10	1.341	1006	0.02288	1.696×10^{-5}	1.680×10^{-5}	1.252×10^{-5}	0.7387
0	1.292	1006	0.02364	1.818×10^{-5}	1.729×10^{-5}	1.338×10^{-5}	0.7362
5	1.269	1006	0.02401	1.880×10^{-5}	1.754×10^{-5}	1.382×10^{-5}	0.7350
10	1.246	1006	0.02439	1.944×10^{-5}	1.778×10^{-5}	1.426×10^{-5}	0.7336
15	1.225	1007	0.02476	2.009×10^{-5}	1.802×10^{-5}	1.470×10^{-5}	0.7323
20	1.204	1007	0.02514	2.074×10^{-5}	1.825×10^{-5}	1.516×10^{-5}	0.7309
25	1.184	1007	0.02551	2.141×10^{-5}	1.849×10^{-5}	1.562×10^{-5}	0.7296
30	1.164	1007	0.02588	2.208×10^{-5}	1.872×10^{-5}	1.608×10^{-5}	0.7282
35	1.145	1007	0.02625	2.277×10^{-5}	1.895×10^{-5}	1.655×10^{-5}	0.7268
40	1.127	1007	0.02662	2.346×10^{-5}	1.918×10^{-5}	1.702×10^{-5}	0.7255

- Span/depth = 0.2*c/20% chord length
- Edge mesh:
 - “Average element size” as $c/128 = 0.002734375$
- “Edge Layer”
 - “First layer thickness” to $c/10,000 = 3.5e-5$
 - “Total number of layers to 24 & “Growth method” to ‘Constant’ & “Growth rate” to 1.2 & “Termination policy” to ‘Truncate’ & toggle on “Enable surface mesh modification”
- Rectangular Refinement Zone
 - Average element size = $c/128 = 0.002734375$
- “Surface”
 - “Maximum element size”

- 2.5 c side = 0.875
 - 0.3 c deep = 0.105
 - 1 c up = 0.35
- Extrusion Mesh
 - Set “Element Size Along Extrusion” to $c/10 = 0.1c = 0.0254$ & “Element Type” to ‘Quads’
 - (note: 2 elements in depth, 2 elements in
- Volume Mesh
 - Set “Maximum element size” to $c = 0.35$
- Boundary Mesh:
 - First layer thickness = $c/256 = 0.0013671875$ m
 - Total number of layers = 10
 - Set Growth method to Constant
 - Growth rate = 1.25
 - Termination policy = Truncate

Goals:

The lift and drag forces will be obtained from the Hypermesh CFD integrated force results in the x,y,z directions. In order to obtain our lift and drag coefficients, the integrated force data must be exported to acusolve where it can be solved for those components.

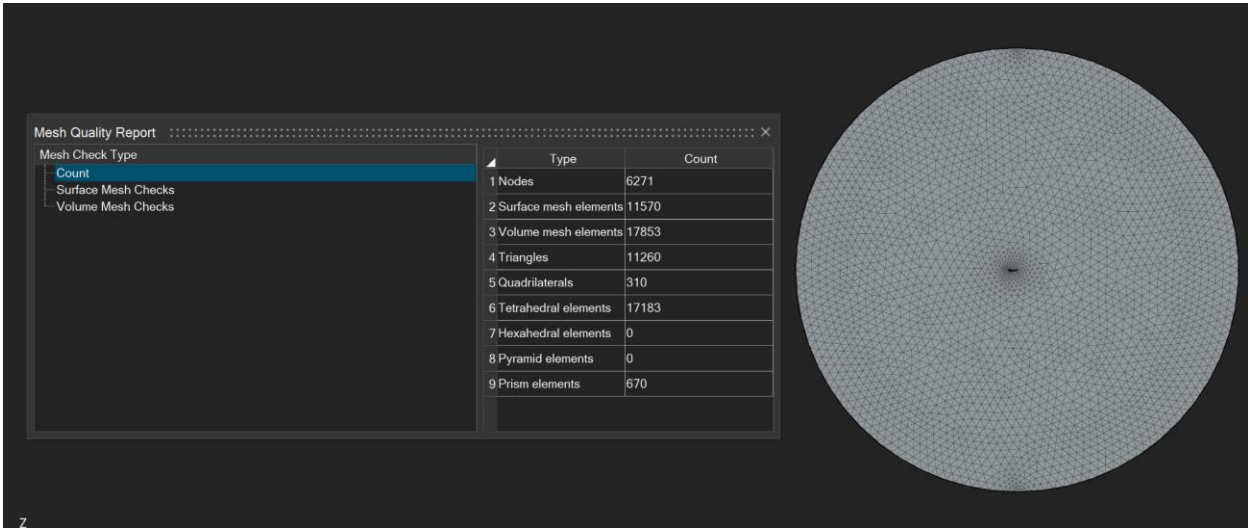
- Lift coeff.
- Drag coeff.
- Pressure coeff.
- Downforce will be calculated to evaluate how effectively the wing enhances grip.
- skin friction
- shear forces on the airfoil’s surface

Questions/Comments for the meetup:

- Steady analysis? What kind of unsteady could we maybe do?
- This is the airfoil we chose
 - Considering stacking for final
- 2D for midterm, then 3D for final
- Farfield with diameter 50x chord
- Having issues with geometry low-poly even though we splined

DEMOS:

- 3
- 7.1



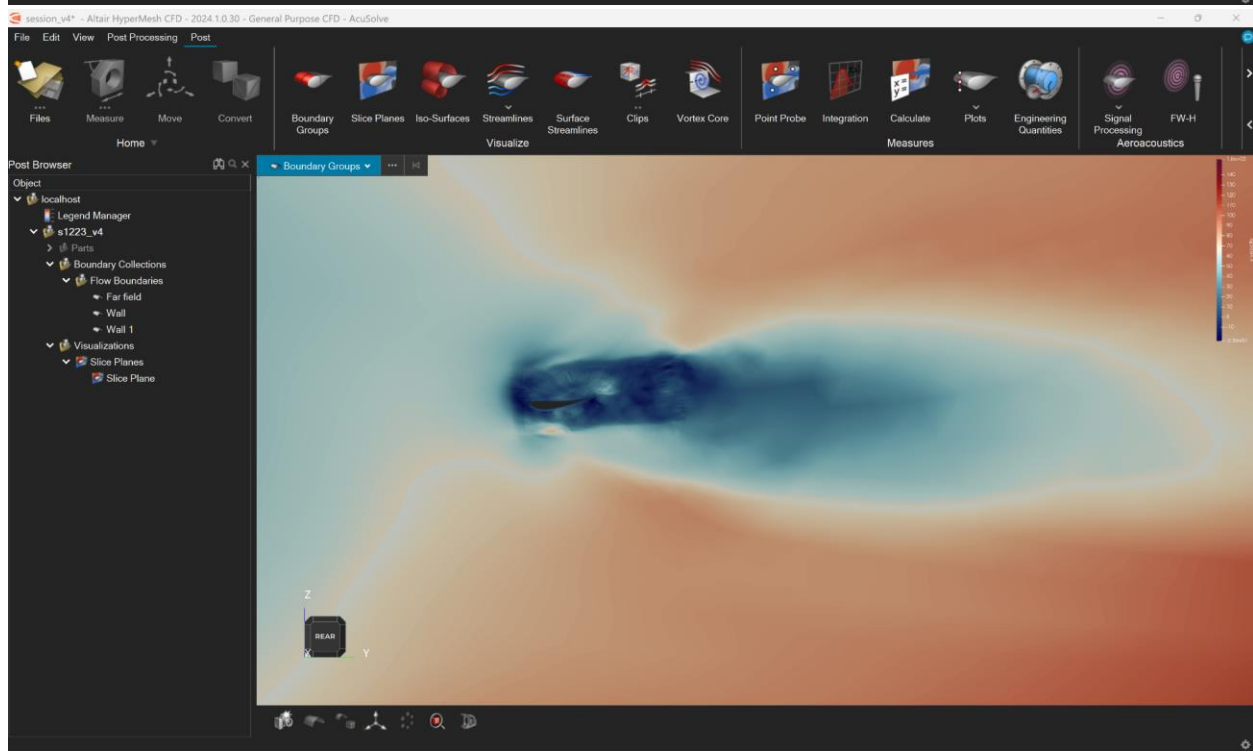
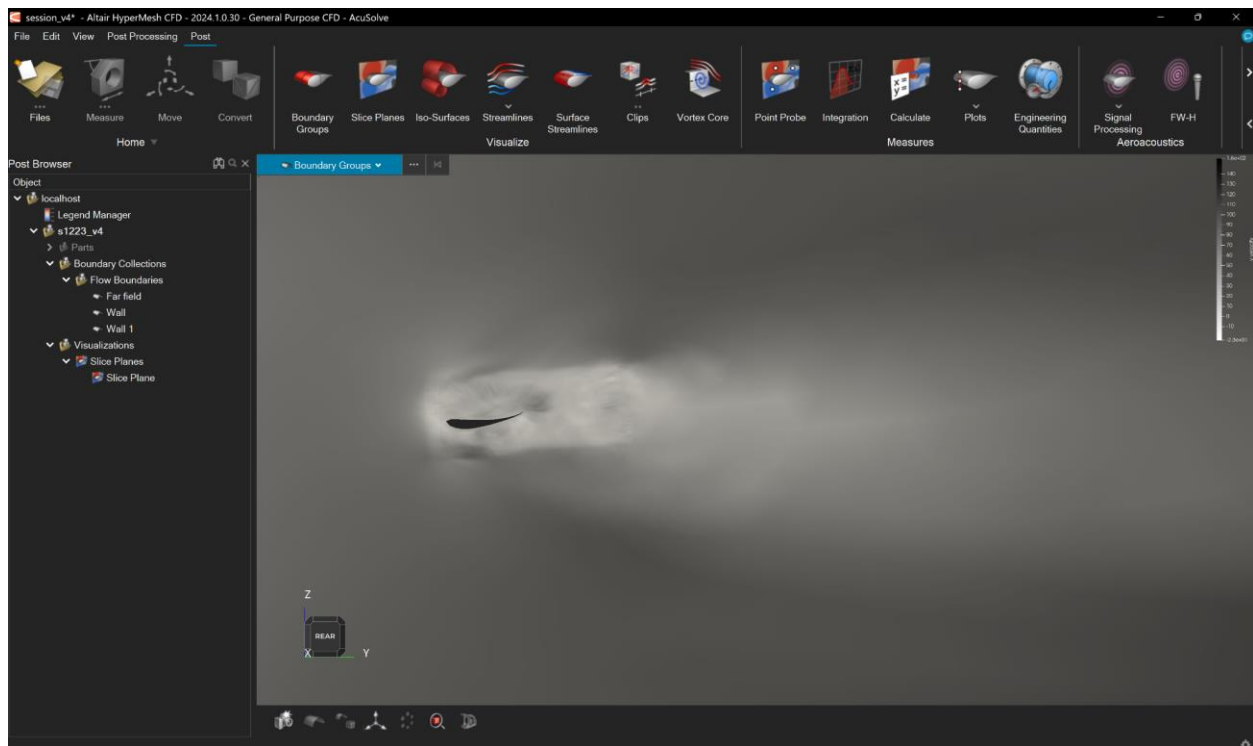
Resources:

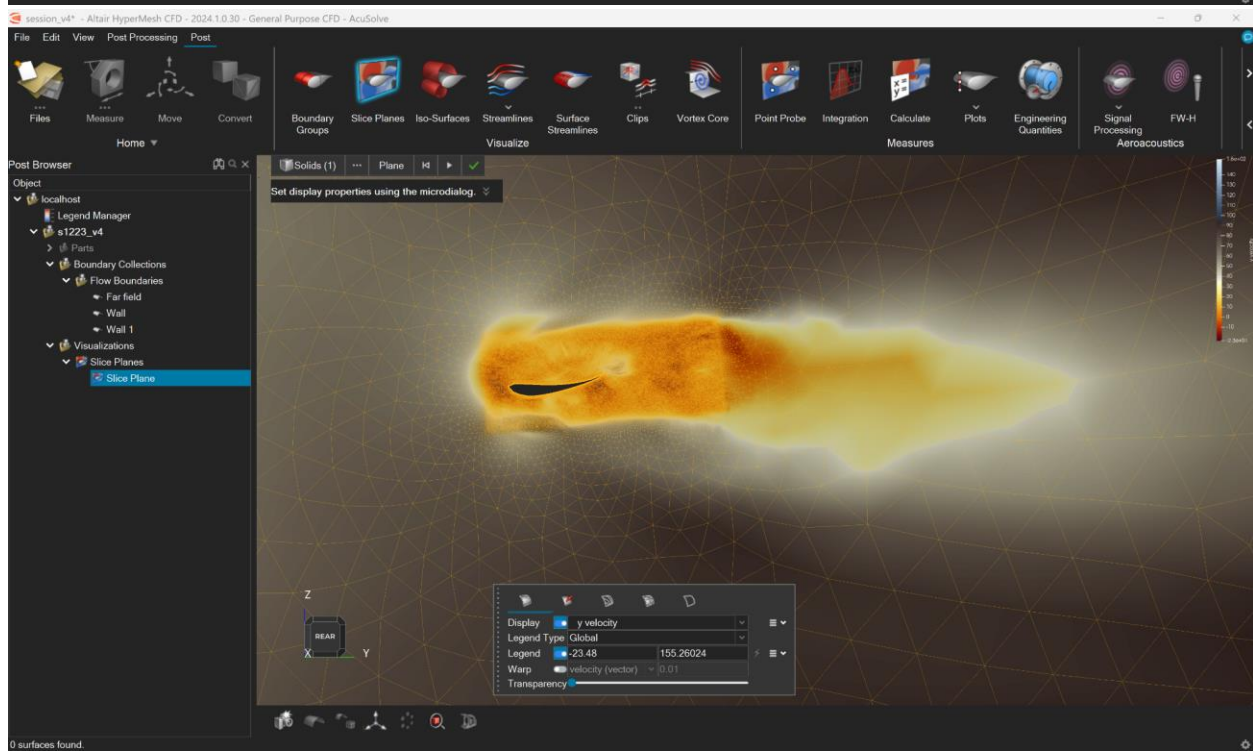
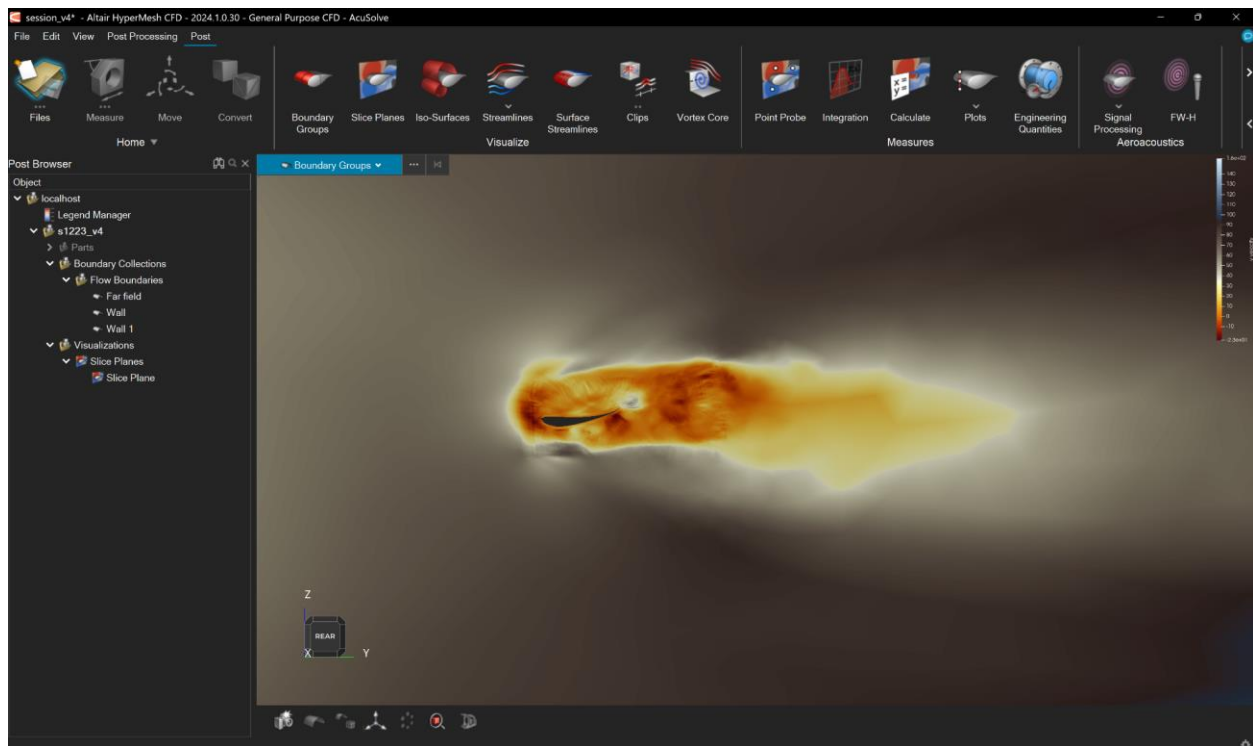
1. https://www.engineersedge.com/physics/viscosity_of_air_dynamic_and_kinematic_14483.htm

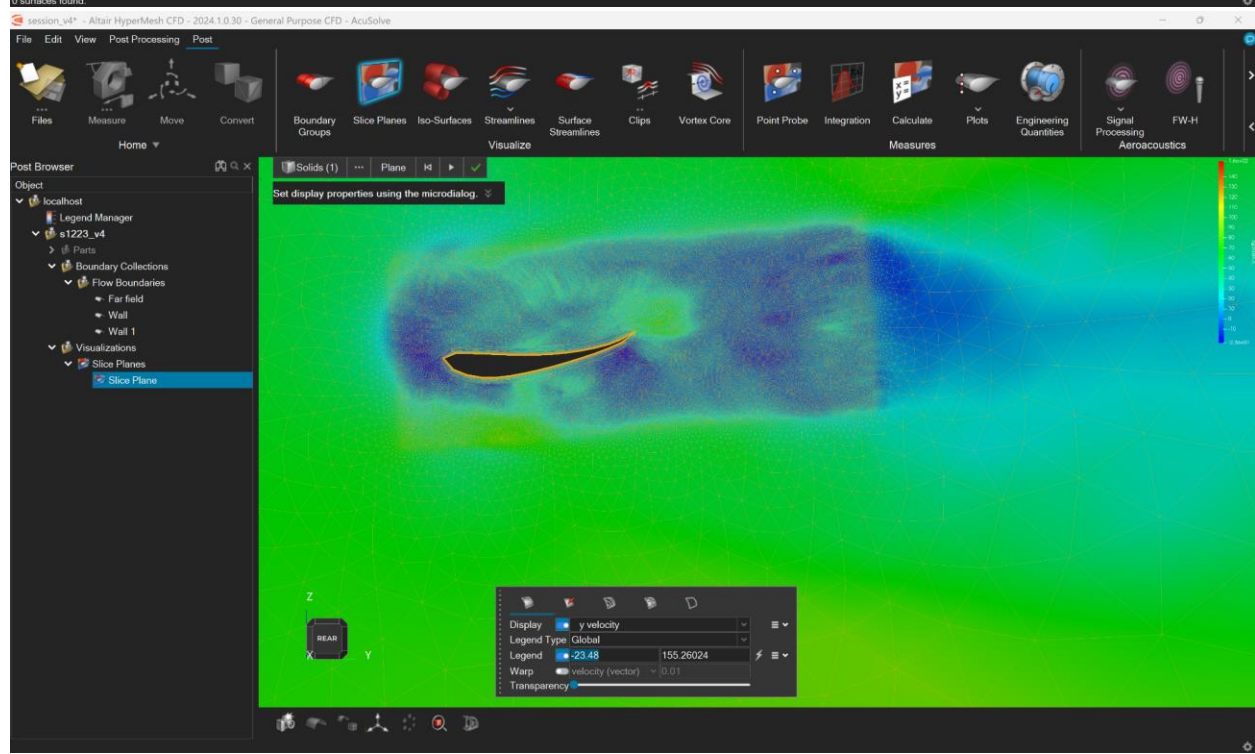
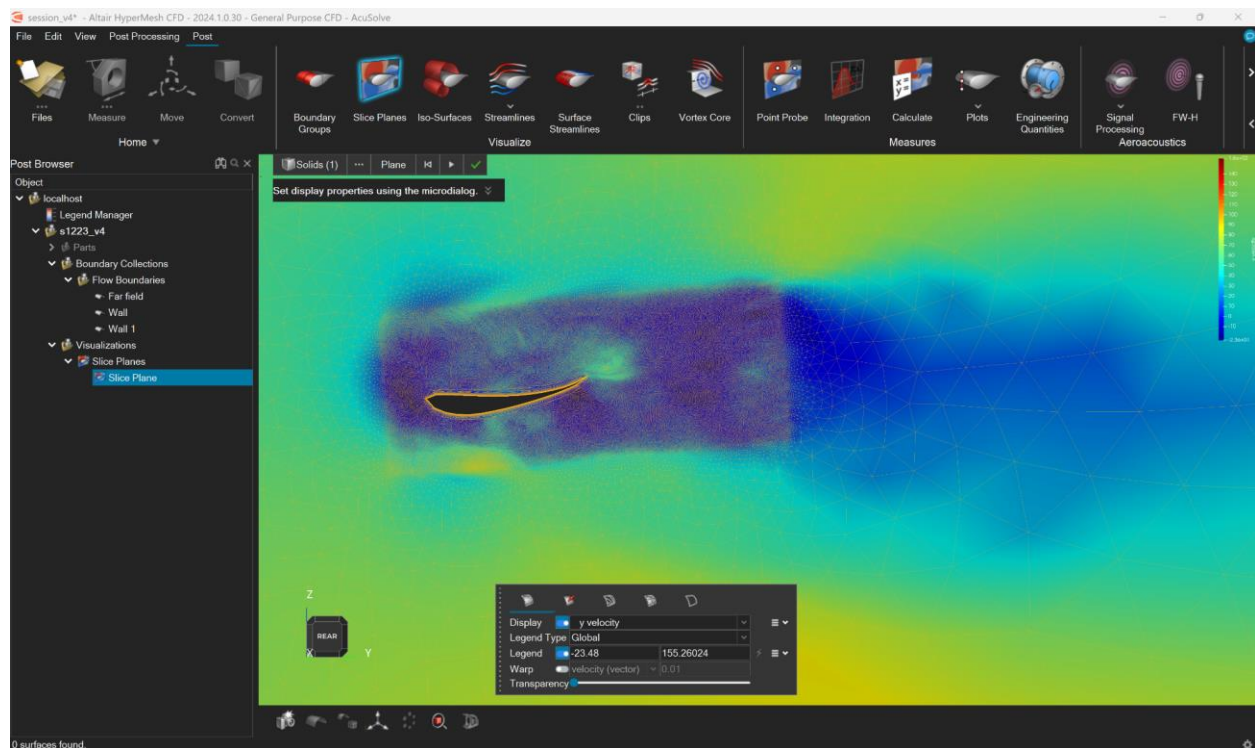
<https://community.altair.com/discussion/21027/how-i-know-drag-force-downforce-drag-coefficient-and-lift-coefficient-from-cfd-analysis-in-hyperworks-cfd>

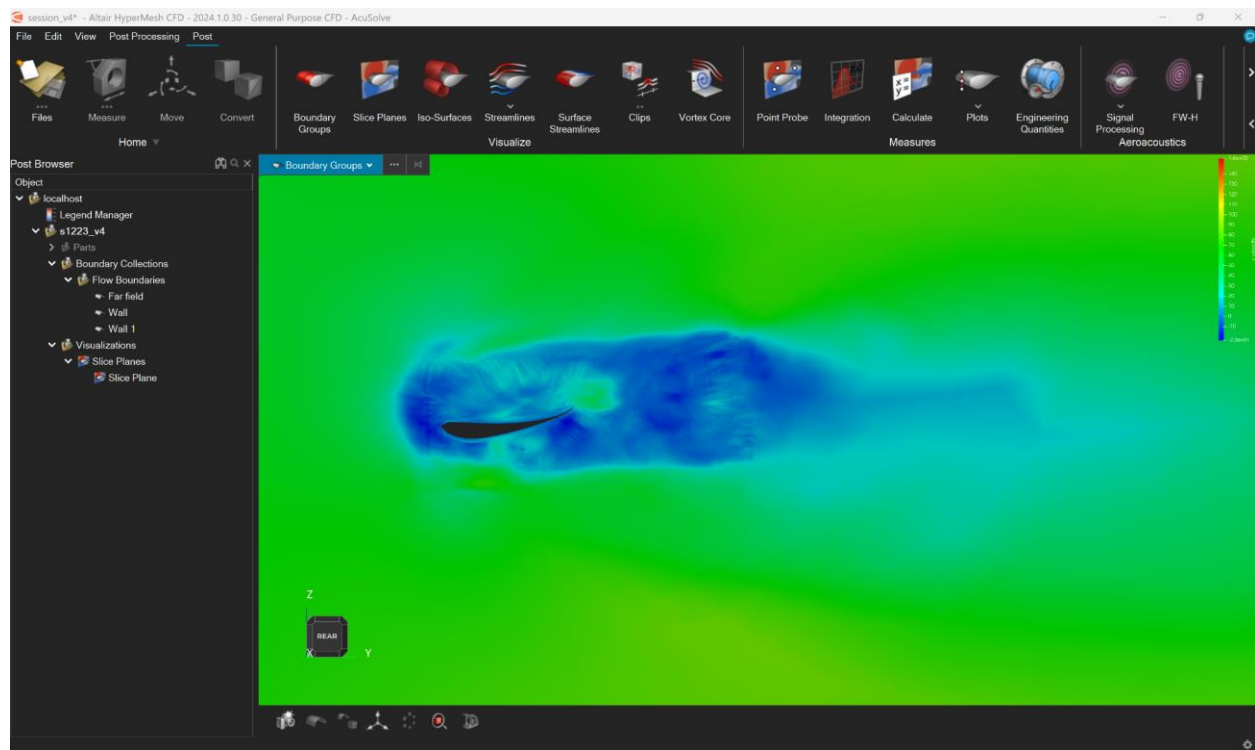
Stacked for final

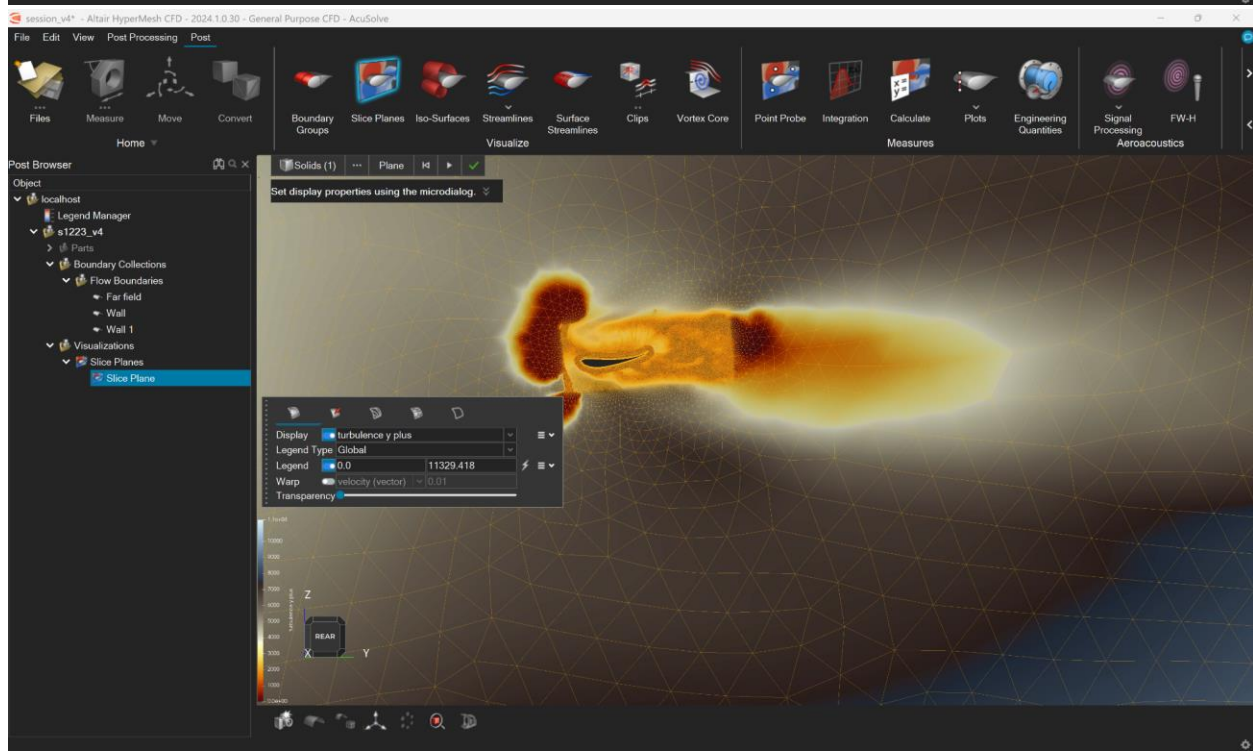
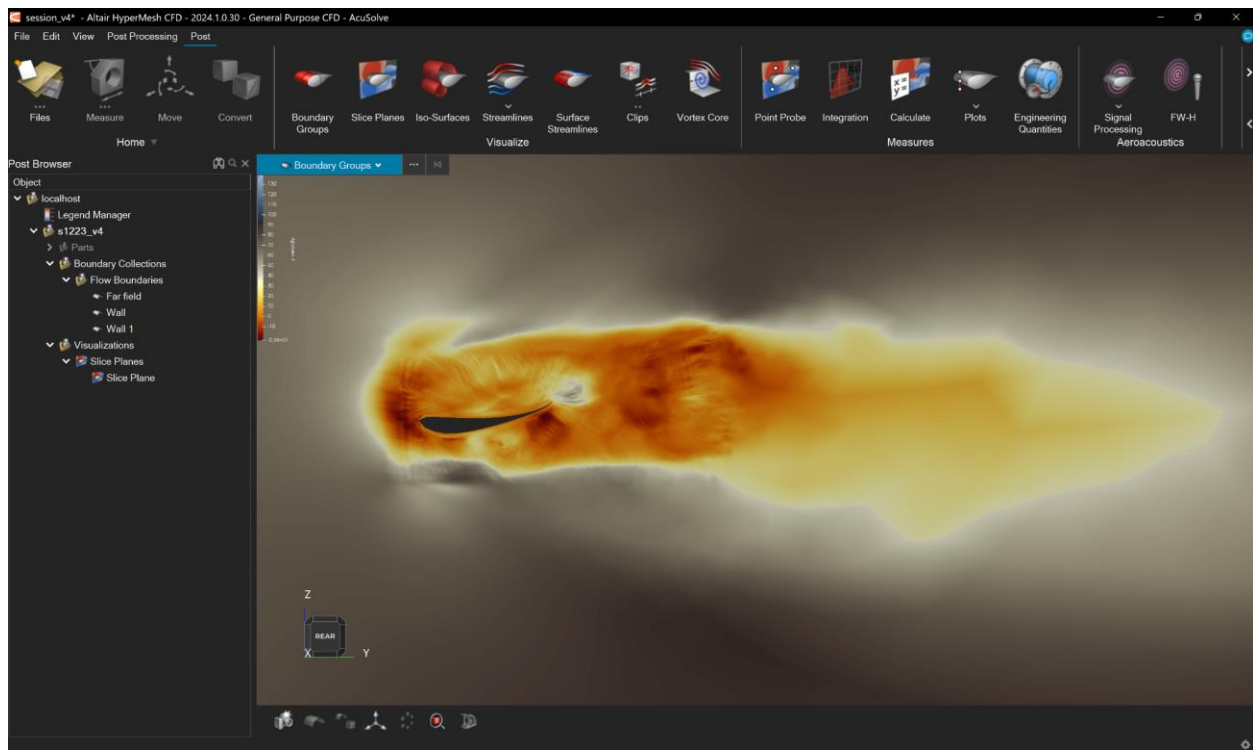
images

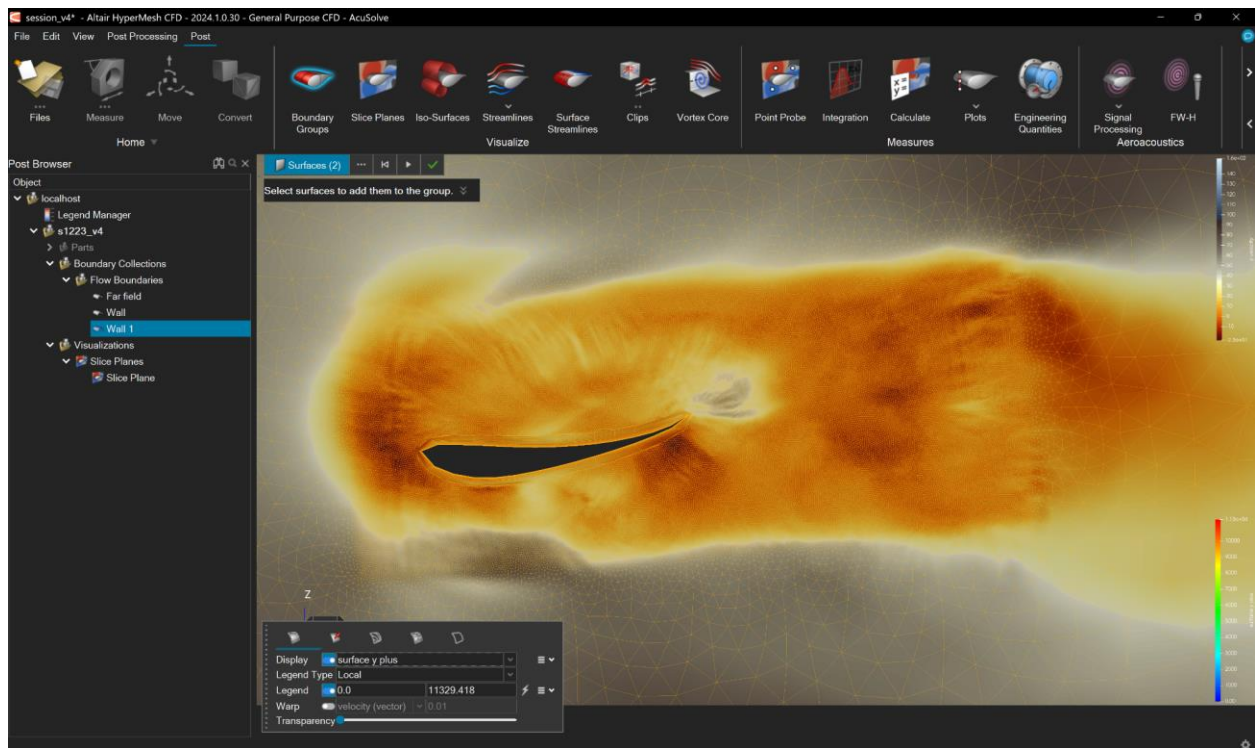


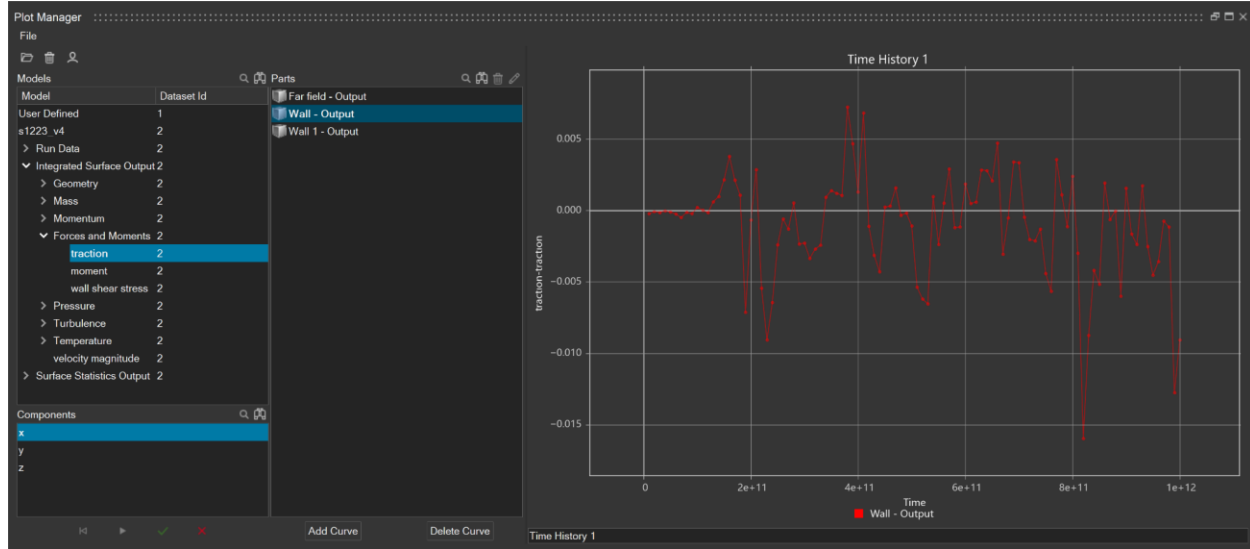
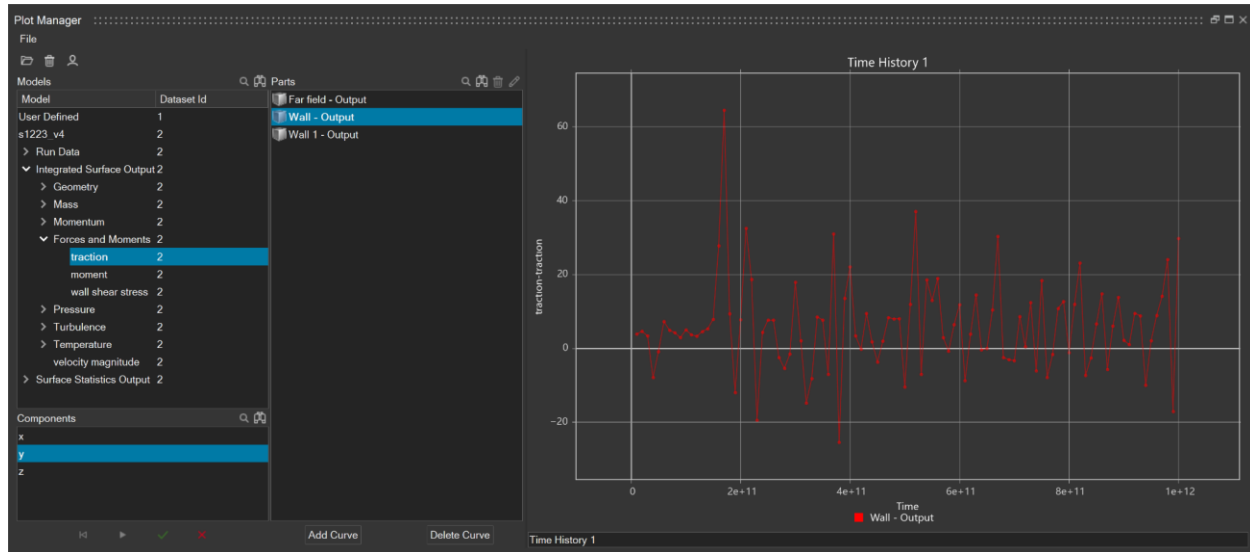


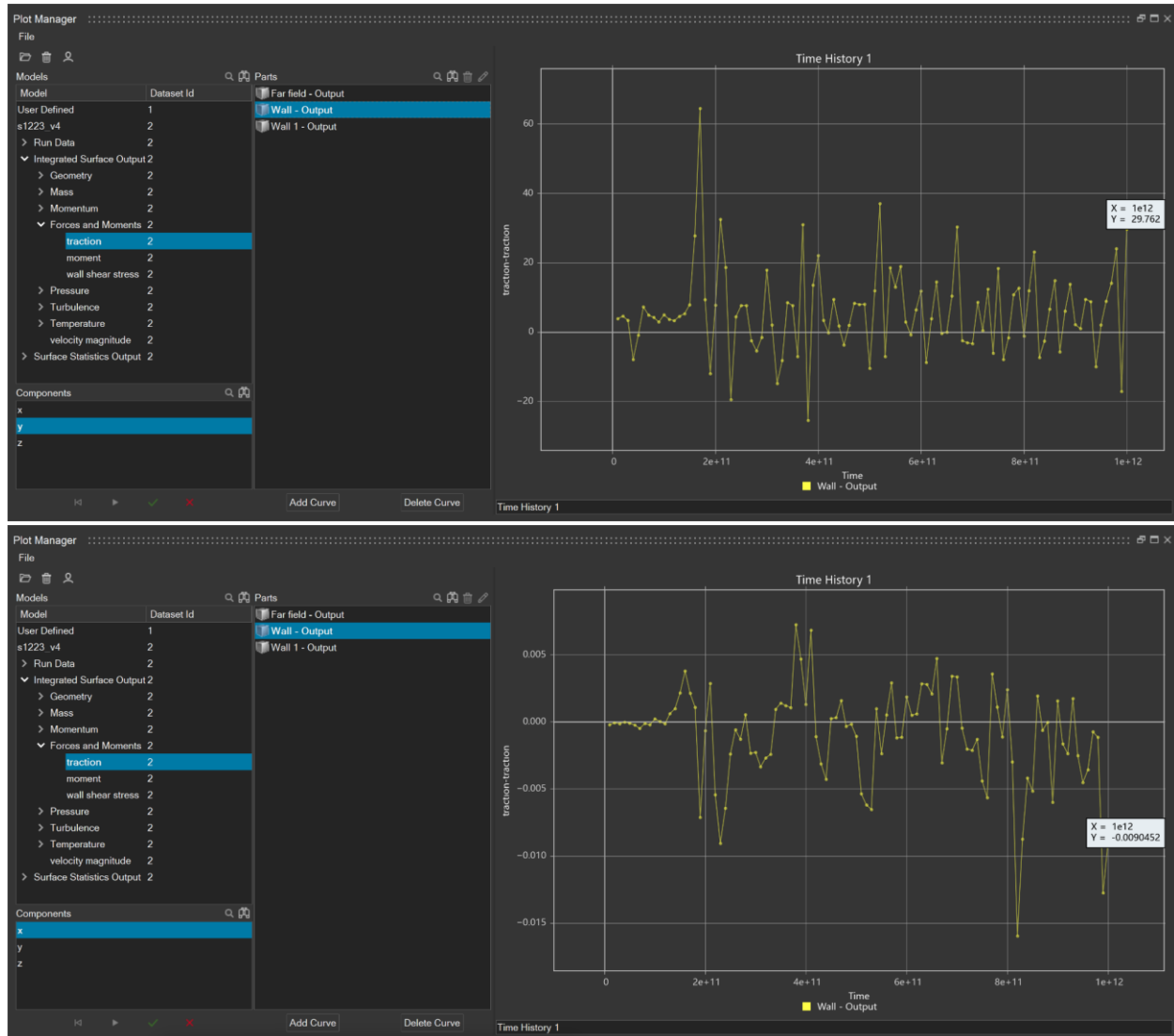












Misc

Summarize findings.

Either : Lowkey our results are garbage, say that in a nice way.

OR

After multiple attempts, it converged

This initial simulation serves as a preliminary overview of expected results before conducting more accurate and computationally intensive simulations for the final project. Future simulations will

For sec 5:

(post-processing, e.g., slices, force plots, streamlines, surface y plus)

GET LIFT, DRAG, PRESSURE slice plots

SURFACE Y PLUS NEEDED

Streamline is a plus